



Available online at www.sciencedirect.com

ScienceDirect

Comput. Methods Appl. Mech. Engrg. 372 (2020) 113312

Computer methods in applied mechanics and engineering

www.elsevier.com/locate/cma

Adaptive hyper reduction for additive manufacturing thermal fluid analysis

Ye Lu, Kevontrez Kyvon Jones, Zhengtao Gan, Wing Kam Liu*

Department of Mechanical Engineering, Northwestern University, Evanston, USA

Received 25 June 2020; received in revised form 16 July 2020; accepted 21 July 2020

Available online xxxx

Abstract

Thermal fluid coupled analysis is essential to enable an accurate temperature prediction in additive manufacturing. However, numerical simulations of this type are time-consuming, due to the high non-linearity, the underlying large mesh size and the small time step constraints. This paper presents a novel adaptive hyper reduction method for speeding up these simulations. The difficulties associated with non-linear terms for model reduction are tackled by designing an adaptive reduced integration domain. The proposed online basis adaptation strategy is based on a combination of a basis mapping, enrichment by local residuals and a gappy basis reconstruction technique. The efficiency of the proposed method will be demonstrated by representative 3D examples of additive manufacturing models, including single-track and multi-track cases. © 2020 Elsevier B.V. All rights reserved.

Keywords: Additive manufacturing; Thermal CFD; Hyper reduction; Adaptivity; Gappy reduced basis learning

1. Introduction

Additive manufacturing has gained tremendous research interests over the last decades for its abilities to manufacture products with complex geometries which are difficult for standard manufacturing processes. However, the lack of reproducibility of the additively manufactured pieces limits its application to real engineering scenario. Numerical simulations have become an essential tool to study the process–structure–properties linkages in this manufacturing process [1].

Numerical models of additive manufacturing, including laser or electron beam powder bed fusion and directed energy deposition, have been developed for accounting for the physics and mechanisms across different scales. Macroscopic part-scale models (e.g. [2–4]) usually consider the thermo-mechanical coupling to study the mechanical properties of final pieces (e.g. residual stresses). In these models, the strong interaction between heat transfer and fluid flow is usually neglected. An equivalent volumetric heat source model calibrated against experiments is usually applied to represent the interaction between the beam and the materials. In addition, the thermal problem can be solved prior to the mechanical problem, for predicting the temperature. Hence, such computations (especially the temperature prediction) are relatively cheap to perform, compared to fine scale models. Models accounting for finer

E-mail addresses: ye.lu@northwestern.edu (Y. Lu), KevontrezJones2021@u.northwestern.edu (K.K. Jones), zhengtao.gan@northwestern.edu (Z. Gan), w-liu@northwestern.edu (W.K. Liu).

^{*} Corresponding author.

scale effects [5–8], e.g. the melt pool formation and materials solidification, are computationally expensive, due to the high non-linearity induced by the thermal-fluid interaction and the underlying small time steps constraints. Therefore, these models are usually considered for studies on relatively small scale phenomena over a short time range, rather than for large part-scale predictions. However, it has been shown that accounting for the fine scale effects is crucial for an accurate prediction of the temperature field (e.g. [9]), which significantly affects the subsequent micro-structure evolution and macroscopic mechanical properties. From this perspective, a part-scale thermal-fluid analysis should be ideal for accurate macroscopic mechanical predictions. Furthermore, if parametric studies are required to study the influence of the process parameters on the fine scale phenomena or macro-scale properties, these models have to be run repetitively, which leads to a prohibitive cost. Hence, reducing the computational cost of the numerical models is desired for studying the additive manufacturing process. In this work, we focus on the thermal fluid flow analysis.

In recent years, model order reduction has become one of the key techniques to reduce the computational cost of numerical simulations. Projection based model reduction methods, like proper orthogonal decomposition (POD) [10–12] and proper generalized decomposition (PGD) [13–15], are based on the assumption of separability of state variables. The separated representation of variables results in the so-called reduced basis, which is expected to be very small compared to the original model size and hence expands a novel reduced solution subspace for original problems. Depending on the solution strategy, the reduced basis can be found either offline from a database computed with full order models (e.g. POD), or on-the-fly by solving the reduced order models (e.g. PGD). The separability of state variables (i.e. reducibility) depends on the specific problems and dominates the efficiency of the reduced order models. These methods are found more successful with linear problems. Nonlinear model reduction usually requires additional techniques to deal with the difficulties induced by nonlinear terms or to improve the reducibility of problems. For example, in order to deal with hyperelasticity problems, asymptotic numerical methods, in conjunction with POD and PGD [16,17], have been used to minimize the necessity of reconstruction of tangent stiffness matrix in the Newton procedure, which is generally the most time-consuming operation in the nonlinear solver. Other techniques devoted to the same idea but considering a partial evaluation of stiffness matrix are missing point estimation [18], hyper reduction [19], and discrete empirical interpolation method [20]. A algorithmic comparison of these methods can be found in [21].

In the context of additive manufacturing or related processes (e.g. welding), model reduction becomes even more challenging, due to the multi-physics coupling, the high non-linearity and the lack of reducibility induced by the moving heat source. Many attempts have been made for macroscopic thermal analysis. In order to improve the reducibility of the problem, a moving frame formulation [22–25] is usually considered, in which the temperature field is computed for a local moving domain attached to the heat source. Some attempts for the thermo-mechanical modeling using non-intrusive model reduction methods are also based on a similar concept [26–29]. However, the moving frame formulation needs assumptions in the boundary of the local domain and its extension to variable loading paths seems difficult. In addition, the thermal analysis is relatively simplified in these works, interactions with the fluid flow are not taken into account.

In this work, we consider a strongly coupled thermal-fluid problem and propose an alternative to deal with it, based on a fixed frame formulation. For tackling the non-linearity, we consider a hyper reduction technique, since it is less intrusive among different nonlinear model reduction methods [21] and therefore its implementation to an existing research code or software for accounting for other physics should be very easy. For limiting the size of reduced basis, we consider a basis mapping from one time step to another so that the reduced basis can be repetitively used. Standard hyper reduction methods rely on a large database which is expected to cover all possible state evolution paths, therefore the extracted POD basis can be kept constant over the entire time range (e.g. [19,23]). However, this is not suitable for the fixed frame based framework. We propose to use an efficient online basis adaptation strategy, in order to avoid the cost of computing a large database with full order models.

Basis adaptation for reduced order models is usually considered during the offline stage for parametric studies [30,31]. An online adaptation for dynamic data-driven modeling has also been considered [32]. In the context of hyper reduction, online basis adaptation is usually considered to be very expensive, since the full stiffness matrix is required [33]. A different and more efficient adaptation method has been proposed for damage problems in [34], which has potential to be applied to additive manufacturing. But for now, no definitive conclusions have been made.

The adaptation method proposed in this work is significantly different. The idea is to use the residuals of current step to enrich the current reduced basis while restricting the residual evaluation to a reduced domain. This domain

is designed as a reduced integration domain used in the hyper reduced order model. Hence, only a small amount of components in residual vectors has to be evaluated, which results in enhanced efficiency. In addition, since the residual vectors result naturally in a gappy basis, we propose a basis learning technique, via gappy POD, for basis compression and reconstruction. It has been shown that the proposed learning technique plays an essential role in the quality of the hyper reduced order models. Together with the reduced integration domain adaptation, this basis adaptation leads to a novel efficient adaptive hyper reduction method. Numerical examples considering both 3D single-track and multi-track simulations of additive manufacturing will be presented.

This paper is organized as follows. Section 2 presents a nonlinear transient thermal-fluid coupled formulation used in additive manufacturing. Section 3 gives a brief review of POD based model reduction and its limitations will be discussed. Section 4 will present the proposed hyper reduction method as well as the adaptation strategy. The application of the proposed method to the thermal fluid analysis in additive manufacturing will be presented in Section 5. Finally, the paper is closed by some concluding remarks.

2. Problem formulation

2.1. Thermal problem

The heat transfer in additive manufacturing is characterized as a nonlinear transient thermal problem, due to its strong interaction with fluid flow, temperature-dependant material properties, material liquid-solid phase changes and the moving heat source.

Let us consider a fixed domain Ω with the heat flux $\bar{\mathbf{q}}$ on surface $\partial \Omega_{\mathbf{q}}$ and a prescribed temperature \bar{T} on $\partial \Omega_T$. Assuming fluid flows with a velocity \boldsymbol{u} through the domain, the energy balance equation reads then

$$C_p \left[\frac{\partial (\rho T)}{\partial t} + \nabla \cdot (\rho u T) \right] = -\nabla \cdot \mathbf{q} \quad \text{in } \Omega$$
 (1)

where C_p and ρ denote respectively the thermal capacity and the density of materials and can be considered as temperature-dependant. The relation between the temperature and heat flux is given by the Fourier law

$$\mathbf{q} = -\mathbf{k} \cdot \nabla T \tag{2}$$

where k is the thermal conductivity tensor. In isotropic cases, k = kI with I denoting the second-order identity tensor. The boundary conditions, including the heat source, can be written as

$$\begin{cases}
\bar{\mathbf{q}} \cdot \mathbf{n} = -h_c(T - T_0) - \sigma_s \varepsilon (T^4 - T_0^4) + q_{\text{source}} & \text{on } \partial \Omega_q \\
T = \bar{T} & \text{on } \partial \Omega_T
\end{cases}$$
(3)

where h_c denotes the convective heat transfer coefficient, σ_s the Stefan-Boltzmann constant, ε the emissivity, **n** the normal direction of the surface $\partial \Omega_q$, T_0 the initial temperature. The heat source q_{source} can be described in different ways. A Gaussian-type distribution [5] is used in this work

$$q_{\text{source}} = \frac{\epsilon Q \eta}{\pi r_{\star}^{2}} \exp(-\epsilon \frac{x_{b}^{2} + y_{b}^{2}}{r_{\star}^{2}})$$
(4)

where Q denotes the flux intensity, ϵ the intensity factor, η the absorptivity, x_b and y_b the coordinates in the local reference system attached to the moving heat source. r_b is the heat source radius.

The balance equation (1) can be equivalently written in terms of specific enthalpy H

$$\frac{\partial(\rho H)}{\partial t} + \nabla \cdot (\rho \mathbf{u} H) = -\nabla \cdot \mathbf{q} \quad \text{in } \Omega$$
 (5)

In case of solid-liquid phase transitions, the specific enthalpy can be divided into the sensible heat h and the latent heat of fusion ΔH , which reads

$$H = h + \Delta H \tag{6}$$

where we can define the sensible heat as

$$h = \int_0^T C_p dT \tag{7}$$

Substituting (6) into (5) gives the following balance equation

$$\frac{\partial(\rho h)}{\partial t} + \nabla \cdot (\rho u h) = -\nabla \cdot \mathbf{q} - \frac{\partial(\rho \Delta H)}{\partial t} - \nabla \cdot (\rho u \Delta H) \quad \text{in } \Omega$$
 (8)

In this work, the thermal problem is considered with Eq. (8). The vaporization is not taken into account here. Hence, the loss of materials and heat due to vaporization and its effect on the materials composition are neglected. The melt pool region Ω_f can be identified by a liquid volume fraction f_l , which is defined as

$$\begin{cases}
f_l = 0, & \text{if } T \leq T_s \\
f_l = \frac{T - T_s}{T_l - T_s}, & \text{if } T_s < T < T_l \\
f_l = 1, & \text{if } T \geq T_l
\end{cases} \tag{9}$$

where T_s and T_l denote respectively the solidus and liquidus temperature of materials. Therefore, once a temperature field is known, the melt pool can be identified as the region where $f_l > 0$.

2.2. Fluid flow problem

The fluid flow problem is considered for the melt pool Ω_{fl} in the additive manufacturing modeling. The fluid flow can be assumed to be incompressible, laminar and Newtonian. The densities of materials (both liquid and solid) are assumed to be constant except for the buoyance force, i.e. Boussinesq approximation (see e.g. [35]). The top surface of melt pool is assumed flat.

The momentum equation to determine the flow velocity reads

$$\frac{\partial(\rho \boldsymbol{u})}{\partial t} + \nabla \cdot \{\rho \boldsymbol{u}\boldsymbol{u}\} = \mu \nabla^2 \boldsymbol{u} - \nabla p - \frac{180\mu(1 - f_l)^2}{c^2(f_l^3 + \boldsymbol{B})}\boldsymbol{u} + \mathbf{f}_b \quad \text{in } \Omega_{fl}$$
(10)

where μ denotes the viscosity, $\{\cdot\}$ denotes the Dyadic product, \mathbf{f}_b is the body forces, p is the pressure inside the melt pool. f_l is the volume fraction of liquid. c is an approximate primary dendritic spacing which is set to 10^{-6} m. B is a small constant (10^{-3}) used to avoid singularity.

The pressure field p is a priori unknown and should be determined by incorporating the following continuity equation

$$\rho \nabla \cdot \boldsymbol{u} = 0 \quad \text{in } \Omega_{f_i} \tag{11}$$

In this work, the body forces contain only the buoyancy force

$$\mathbf{f}_{b} = \rho_{0} g \beta (T - T_{0}) \mathbf{I} \tag{12}$$

where ρ_0 denotes the reference density at initial temperature T_0 , g the gravitational acceleration, β the thermal expansion coefficient.

The surface tension (i.e. Marangoni force) is considered as shear stress boundary conditions applied to the top surface of melt pool

$$\tau_{x} = \mu \frac{\partial u_{x}}{\partial z} = \frac{d\gamma}{dT} \nabla_{x} T$$

$$\tau_{y} = \mu \frac{\partial u_{y}}{\partial z} = \frac{d\gamma}{dT} \nabla_{y} T$$
(13)

where the γ is the surface tension which depends on both temperature and materials. $\frac{d\gamma}{dT}$ is the temperature coefficient which has usually negative values [5].

Therefore, the driving forces of flow velocity contain only the surface tension and the buoyancy force. We remark that the fluid flow equations are only solved for the melt pool region, whereas the heat transfer equations are solved within the whole domain. The flow velocity outside the melt pool is simply set to zero.

2.3. Conservation formulation

The conservation formulation of the thermal problem and the fluid flow problem can be obtained by integrating the presented balance equations over the domain and is summarized as follows.

• Energy conservation

$$\int_{\Omega} \left(\frac{\partial (\rho h + \rho \Delta H)}{\partial t} + \nabla \cdot (\rho \mathbf{u} h + \rho \mathbf{u} \Delta H) + \nabla \cdot \mathbf{q} \right) dV = 0$$
(14)

• Momentum conservation

$$\int_{\Omega_{f_b}} \left(\frac{\partial (\rho \mathbf{u})}{\partial t} + \nabla \cdot \{ \rho \mathbf{u} \mathbf{u} \} - \mu \nabla^2 \mathbf{u} + \nabla p + \frac{180\mu (1 - f_l)^2}{c^2 (f_l^3 + B)} \mathbf{u} - \mathbf{f}_b \right) dV = 0$$
(15)

• Mass conservation

$$\int_{\Omega_{f_1}} (\rho \nabla \cdot \boldsymbol{u}) \, dV = 0 \tag{16}$$

and subjected to the boundary conditions as described in Eqs. (3) and (13).

2.4. Semi-discretized formulation

The conservation equations can be discretized by a finite volume or stabilized finite element method. In this work, the finite volume method is adopted with a staggered arrangement for flow velocity components, as presented in [36]. The semi-discretized forms of the three conservation equations can be written as

• Energy conservation

$$\frac{\partial \mathbf{h}}{\partial t} + \mathcal{K}(\mathbf{h}, \mathbf{u})\mathbf{h} = \mathbf{Q}(\mathbf{h}, \mathbf{u}, t) \tag{17}$$

• Momentum conservation

$$\frac{\partial \mathbf{u}}{\partial t} + \mathcal{A}(\mathbf{u}, \mathbf{T})\mathbf{u} = \mathbf{F}(\mathbf{u}, \mathbf{T}, \mathbf{p}, t) \tag{18}$$

• Mass conservation

$$\mathbf{M}(\mathbf{u}) = 0 \tag{19}$$

where \mathbf{h} , \mathbf{u} and \mathbf{p} denote respectively the nodal values of entropy, velocity and pressure, and are functions of space \mathbf{X} and time t. \mathcal{K} and \mathcal{A} are the discretized convection-diffusion terms respectively for energy and momentum equations. \mathbf{Q} and \mathbf{F} are discretized source terms which are both functions of state variables (velocity, temperature or entropy) and can vary in time.

This nonlinear thermal-fluid coupled problem can be solved by a linearization technique. This work uses the well-known SIMPLE algorithm [36] incorporated with an implicit scheme for the time integration. The solution procedure of each time step is summarized as follows.

- 1. Initialization for **h**, **u** and **p**.
- 2. Solve the energy equation (17) for **h**.
- 3. Compute the temperature **T** using (7).
- 4. Update the melt pool region.
- 5. Update A and F and solve the momentum equation (18) for u.
- 6. Solve the continuity equation (19) to correct the pressure **p**.
- 7. Correct the velocity **u** with pressure.
- 8. Check the velocity convergence: if convergence, go to step 9, otherwise, return to step 5 for a new u.
- 9. Update K and Q with u and h.
- 10. Check the global energy convergence criterion: if convergence, go to next time step, otherwise, return to step 2 for a new **h**.

Solving this problem is computationally expensive due to the repetitive solution of the underlying equations. The computational expense for constructing the so-called "stiffness" matrix (e.g. \mathcal{K} and \mathcal{A}) and their inversion cost increase quickly with the dimension of the system.

3. Brief review of POD based model reduction and its limitations

Standard POD based model reduction methods rely on an offline-online strategy. The offline stage consists in learning (with data and POD) a reduced basis, deemed "optimal", that is expected to approximate the original solution space. The online stage is a projection procedure in which the original model is mapped to that reduced solution subspace.

As an example, the thermal problem (17) is considered for illustration purposes. The same concept can be applied to the fluid flow problem (18) and (19).

3.1. Proper orthogonal decomposition

Considering a set of sampling data, for example the selected space-time solution of the thermal problem (17) from full order computations: $\mathbf{h}_s = [\mathbf{h}(t_1), \dots, \mathbf{h}(t_s)] \in \mathbb{R}^{n \times s}$, where n stands for the spatial degrees of freedom of the original full order model, the POD attempts to seek an orthogonal projector $\mathbf{\Pi}_{\Phi} = \mathbf{\Phi} \mathbf{\Phi}^T$ that minimizes the following summed projection error with respect to the original data.

$$\boldsymbol{\Phi} = \underset{s,t,\mathbf{Y}^T\mathbf{Y}=\mathbf{I}}{\operatorname{argmin}} \sum_{i=1}^{s} \|\mathbf{h}(t_i) - \mathbf{Y}\mathbf{Y}^T\mathbf{h}(t_i)\|_2^2$$
(20)

The solution of this minimization problem can be obtained by the Singular Value Decomposition (SVD), which reads

$$\mathbf{h}_{c} = \boldsymbol{\Phi} \boldsymbol{\Sigma} \mathbf{V}^{T} \tag{21}$$

where $\Phi = [\Phi^{(1)}, \ldots, \Phi^{(n)}] \in \mathbb{R}^{n \times n}$, $\mathbf{V} = [\mathbf{V}^{(1)}, \ldots, \mathbf{V}^{(s)}] \in \mathbb{R}^{s \times s}$. They are orthogonal bases and represent respectively the variation of data in space and time. $\Sigma \in \mathbb{R}^{n \times s}$ contains the singular values $\sigma^{(i)}$ with $i \leq \min(n, s)$ in decreasing amplitude which can be interpreted as the weights of the different modes. Hence, the projection error with a reduced basis of m modes: $\Phi_m = [\Phi^{(1)}, \ldots, \Phi^{(m)}]$ with $m \leq n$ can be measured by

$$\epsilon_{proj} = \|\mathbf{h}_s - \boldsymbol{\Pi}_{\boldsymbol{\Phi}_m} \mathbf{h}_s\|_F = \sqrt{\sum_{i=m+1}^s \sigma^{(i)}}$$
(22)

where $\|\cdot\|_F$ denotes the Frobenius norm, which is equivalent to the summation error in (20). A problem is said to be reducible if the necessary modes m is small enough for a good accuracy.

3.2. POD Based reduced order model

The POD method can be used to define a reduced solution subspace for the reduced order model. For the sake of stability, we usually take the solution variation $\Delta \mathbf{h}_s$ with respect to a reference value as the original sampling data matrix, the SVD reads then

$$\Delta \mathbf{h}_s = \mathbf{h}_s - \bar{\mathbf{h}}_s = \boldsymbol{\Phi} \boldsymbol{\Sigma} \mathbf{V}^T \tag{23}$$

where $\bar{\mathbf{h}}_s$ can be either the initial or mean value of \mathbf{h} . In a transient problem, this usually takes the initial one. By selecting the most representative modes and assuming the sampling database \mathbf{h}_s is large enough, the reduced basis $\boldsymbol{\Phi}_m$ can be obtained in such a way that the problem solution \mathbf{h} falls into its span, i.e.

$$\operatorname{span}(\mathbf{h} - \bar{\mathbf{h}}) \approx \operatorname{span}(\mathbf{h}_{\varsigma} - \bar{\mathbf{h}}_{\varsigma}) \approx \operatorname{span}(\boldsymbol{\Phi}_{m}) \tag{24}$$

Hence, the following equality holds, if the approximation error is neglected

$$\mathbf{h}(\mathbf{X},t) = \bar{\mathbf{h}}(\mathbf{X}) + \boldsymbol{\Phi}_m(\mathbf{X})\boldsymbol{\alpha}_m(t) \qquad \forall \mathbf{X} \in \Omega$$
 (25)

where $\alpha_m \in \mathbb{R}^m$ is the basis coefficient vector and is a priori unknown.

In what follows, we assume the reduced basis Φ_m is already known for a given level of approximation accuracy by the offline stage. For simplicity, the subscript m is omitted and Φ takes the place of Φ_m . In addition, we adopt the following reduced basis Ψ instead of Φ (as suggested by [23]) with

$$\boldsymbol{\Psi}^{(i)} = \sqrt{\boldsymbol{\sigma}^{(i)}} \, \boldsymbol{\Phi}^{(i)} \tag{26}$$

It can be noticed that $\operatorname{span}(\Psi) = \operatorname{span}(\Phi)$. Hence, Eq. (25) can be written as

$$\mathbf{h}(\mathbf{X},t) = \bar{\mathbf{h}}(\mathbf{X}) + \boldsymbol{\Psi}(\mathbf{X})\boldsymbol{\alpha}(t) \qquad \forall \mathbf{X} \in \Omega$$
 (27)

Now, we can define a reduced order model for the reference problem (17), which reads

$$\boldsymbol{\Psi}^{T} \boldsymbol{\Psi} \frac{\partial \boldsymbol{\alpha}}{\partial t} + \boldsymbol{\Psi}^{T} \mathcal{K}(\mathbf{h}, \mathbf{u}) \boldsymbol{\Psi} \boldsymbol{\alpha} = \boldsymbol{\Psi}^{T} \mathbf{Q}(\mathbf{h}, \mathbf{u}, t) - \boldsymbol{\Psi}^{T} \mathcal{K}(\mathbf{h}, \mathbf{u}) \bar{\mathbf{h}}$$
(28)

or equivalently

$$\boldsymbol{\Psi}^{T} \boldsymbol{\Psi} \frac{\partial \boldsymbol{\alpha}}{\partial t} + \mathcal{K}_{r}(\mathbf{h}, \mathbf{u}) \boldsymbol{\alpha} = \mathbf{Q}_{r}(\mathbf{h}, \mathbf{u}, t, \bar{\mathbf{h}})$$
(29)

where $K_r \in \mathbb{R}^{m \times m}$ and $\mathbf{Q}_r \in \mathbb{R}^m$, whereas $K \in \mathbb{R}^{n \times n}$ and $\mathbf{Q} \in \mathbb{R}^n$. Recalling that n is the spatial degrees of freedom of the full order model, the mode number m is generally very small compared to $n: m \ll n$. Therefore, the system for solving the unknown basis coefficient α is significantly reduced. The original problem solution can be reconstructed using Eq. (27), once α is obtained.

3.3. Discussion on the limitations

The presented POD based reduced order model works well when the problem is linear, in which the so-called "stiffness" matrix \mathcal{K} can be constructed once for all during the computations. Instead of solving a large number n of system equations, we solve only a small reduced system of dimension $m \ll n$. The speedup is usually significant, thanks to the reduced inversion cost.

In nonlinear cases, \mathcal{K} depends on the state variables of the system (e.g. h, u), \mathcal{K} (or sometimes a tangent stiffness matrix) should be repetitively updated in an iterative scheme. Consequently, the main computational cost of the numerical model is devoted to the construction of \mathcal{K} , which results in a low efficiency of the reduced order model.

Another drawback of this method is that the offline-computed reduced basis Ψ is needed to be well representative of the solution space. Otherwise, the solution computed by the reduced order mode is inaccurate. This implies the necessity of a very large database which covers all the possible loading and boundary conditions as well as the possible evolution of material properties. This kind of database is usually difficult to obtain.

These challenges are crucial for its application to additive manufacturing simulations. The highly nonlinear and transient aspects of the underlying problem make the standard POD approaches inappropriate. In addition, the moving heat source further challenges the reducibility of the underlying problem, although some of the issues can be overcome by considering a steady state assumption with a moving frame formulation (e.g. [26,23]).

4. Hyper reduced order modeling with online reduced basis learning

This section presents a hyper model reduction method enhanced by an efficient online reduced basis learning technique, in order to overcome the previously mentioned difficulties associated with POD based model reduction methods.

4.1. Hyper model reduction

The hyper model reduction method is designed for the purpose of reducing the \mathcal{K} -matrix construction cost for nonlinear problems. The basic idea is to introduce a reduced integration domain (RID), denoted by Ω_{RID} , so that only a small amount of the stiffness-matrix components are needed to be computed. This idea is based on the observation that the POD reduced order model (29) requires only a small number of balance equations to make the system solvable. Theoretically, in order to have a well conditioned stiffness-matrix $\mathcal{K}_r = \Psi^T \mathcal{K} \Psi \in \mathbb{R}^{m \times m}$, we only need an original stiffness-matrix $\mathcal{K} \in \mathbb{R}^{n \times n}$ of rank l with $m \le l \le n$. This observation allows us to compute partially the necessary components of \mathcal{K} , instead of performing a full construction. Hence, the computational cost can be reduced by selecting appropriately the components of the discretized balance equations (29).

Selecting the components of balance equations is equivalent to design a RID. It has been shown that the RID selection is crucial for hyper reduction methods [23,37] in terms of accuracy and efficiency. For now, we assume a RID is already selected for our problems. The proposed selection technique will be presented later in following subsections.

Now, let $\mathbf{L} \in \mathbb{R}^{l \times n}$ be a selection matrix with $m \leq l \leq n$. Each line of \mathbf{L} contains only a nonzero component (equals to 1) in the selected position. The problem solution in the RID reads then

$$\mathbf{h}_{RID}(\mathbf{X}, t) = \mathbf{L}\mathbf{h}(\mathbf{X}, t) = \mathbf{L}\mathbf{\bar{h}}(\mathbf{X}) + \mathbf{L}\boldsymbol{\Psi}(\mathbf{X})\boldsymbol{\alpha}(t) \qquad \forall \mathbf{X} \in \Omega_{RID}$$
(30)

where $\mathbf{h}_{RID} \in \mathbb{R}^l$, $\boldsymbol{\Psi}$ is a reduced basis obtained from a database \mathbf{h}_s . It is obvious that \mathbf{h}_{RID} obeys the energy balance in Ω_{RID} . $\bar{\mathbf{h}}$ denotes the initial state in this work. Hence, substituting \mathbf{h} by \mathbf{h}_{RID} in Eq. (17) and multiplying both sides by the hyper reduced basis function $(\mathbf{L}\boldsymbol{\Psi})^T$ give

$$\boldsymbol{\Psi}^{T}\mathbf{L}^{T}\mathbf{L}\boldsymbol{\Psi}\frac{\partial\boldsymbol{\alpha}}{\partial t} + \boldsymbol{\Psi}^{T}\mathbf{L}^{T}\mathbf{L}\boldsymbol{\mathcal{K}}(\mathbf{h},\mathbf{u})\boldsymbol{\varPsi}\boldsymbol{\alpha} = \boldsymbol{\varPsi}^{T}\mathbf{L}^{T}\mathbf{L}\mathbf{Q}(\mathbf{h},\mathbf{u},t) - \boldsymbol{\varPsi}^{T}\mathbf{L}^{T}\mathbf{L}\boldsymbol{\mathcal{K}}(\mathbf{h},\mathbf{u})\bar{\mathbf{h}}$$
(31)

or equivalently,

$$\boldsymbol{\Psi}^{T} \mathbf{W} \boldsymbol{\Psi} \frac{\partial \boldsymbol{\alpha}}{\partial t} + \boldsymbol{\Psi}^{T} \mathbf{W} \mathcal{K}(\mathbf{h}, \mathbf{u}) \boldsymbol{\Psi} \boldsymbol{\alpha} = \boldsymbol{\Psi}^{T} \mathbf{W} \mathbf{Q}(\mathbf{h}, \mathbf{u}, t) - \boldsymbol{\Psi}^{T} \mathbf{W} \mathcal{K}(\mathbf{h}, \mathbf{u}) \bar{\mathbf{h}}$$
(32)

where $\mathbf{W} = \mathbf{L}^T \mathbf{L} \in \mathbb{R}^{n \times n}$ is a symmetric indicator matrix with 1 in selected diagonal components. This is the hyper reduced order model to the problem (17). Again, the unknown variable of the reduced order system is the basis coefficient $\boldsymbol{\alpha}$. The original problem solution \mathbf{h} can be found using Eq. (27). Unlike the standard POD reduced order model (29), the stiffness-matrix $\boldsymbol{\mathcal{K}}$ of the nonlinear system is computed or updated only for selected useful components, thanks to the introduction of the indicator matrix \mathbf{W} . Hence, the computational cost is further reduced, compared to standard POD reduced order models. This is also why the method is referred to as hyper model order reduction or simply hyper reduction.

The efficiency of the method depends essentially on the choice of RID and the quality of reduced basis. A large RID can lead to a good precision and meanwhile a high computational cost. The quality of the reduced basis strongly depends on the reducibility of the underlying problem, which is directly related to the loading condition and the problem description, etc. Therefore, these aspects become the most essential parts of a hyper reduction method, especially when dealing with complex multi-physics problems, like additive manufacturing. In what follows, a systematic adaptive hyper reduction framework is presented, dedicated to modeling a transient nonlinear multi-physics problem with a concentrated moving source.

4.2. Reduced integration domain design

In general, the RID should be able to capture the most relevant variations of state variables in the solution domain. In the hyper reduced order model, this information is stored inside the reduced basis Ψ . Denoted by Ω_{RB} , the sub-domain containing the most relevant information of reduced basis can be defined as

$$\Omega_{RB} = \{ \mathbf{X} \in \Omega \mid \|\nabla \boldsymbol{\varPsi}^{(i)}(\mathbf{X})\| \ge c_{RB} \max_{\mathbf{X}} \|\nabla \boldsymbol{\varPsi}^{(i)}(\mathbf{X})\| \}, \quad \forall i = 1, \dots, m$$
(33)

where c_{RB} is a small threshold. In general, higher order derivatives can be adopted. This work uses the gradient, as a first attempt. The derivatives are computed by a finite difference method.

In addition, the sub-domain containing the relevant boundary conditions and the external loading should be included in the RID. Denoted by Ω_{BC} , this sub-domain can be defined as

$$\Omega_{BC} = \{ \mathbf{X} \in \Omega \mid |\mathbf{Q}(\mathbf{X})| \ge c_{BC} \max_{\mathbf{X}} |\mathbf{Q}(\mathbf{X})| \}$$
(34)

Similarly, c_{BC} is a small threshold but not necessarily the same as c_{RB} . Since the problem is multi-physically coupled, the relevant interaction domain should be included. In this work, the melt pool region should be the relevant sub-domain for the thermal fluid interaction.

$$\Omega_{f_l} = \{ \mathbf{X} \in \Omega \mid f_l(\mathbf{X}) > 0 \} \tag{35}$$

Hence, the basic reduced integration domain can be defined as

$$\Omega_{RID} = \Omega_{RB} \cup \Omega_{BC} \cup \Omega_{f_l} \tag{36}$$

4.3. Reduced basis design and enrichment

The most challenging issue induced by a moving source for model reduction is the lack of problem reducibility in the standard fixed frame. The concept of similarity in problem solutions from one time step to another is not straightforwardly applicable. The reduced basis Ψ cannot be kept constant over the entire time range, unless a very large sampling database: \mathbf{h}_s (23) is available from the offline stage. This problem is usually addressed by considering a moving frame formulation (e.g. [26,23,22,27,28]), in which the moving source becomes a fixed one in a local moving domain. However, this kind of approaches needs assumptions on the boundary of the local domain and its generalization to variable loading paths seems difficult.

In this work, we rely on a fixed frame formulation. Hence, the reduced basis design becomes an adequate task to make the problem reducible. The proposed technique to deal with the problem is a combination of reduced basis mapping and enrichment.

Inspired by the moving frame formulation, we consider that the similarity of problem solutions around the moving source exists and is captured by a reduced basis mapping. Let t_n and t_{n+1} be two different time steps, the reduced basis mapping $\mathcal{M}: \mathbb{R}^{n \times m} \to \mathbb{R}^{n \times m}$ is defined as a translation in the moving direction, which reads

$$\begin{cases}
\boldsymbol{\Psi}^{0}(\mathbf{X}; t_{n+1}) = \boldsymbol{\Psi}(\mathbf{X} - \mathbf{v}\Delta t; t_{n}), & \text{if } \mathbf{X} - \mathbf{v}\Delta t \in \Omega \\
\boldsymbol{\Psi}^{0}(\mathbf{X}; t_{n+1}) = \boldsymbol{\Psi}(\mathbf{X}; t_{n}), & \text{if } \mathbf{X} - \mathbf{v}\Delta t \notin \Omega
\end{cases}$$
(37)

where Ψ^0 denotes the initial reduced basis after mapping, \mathbf{v} denotes the velocity of the moving source and $\Delta t = t_{n+1} - t_n$. This is the simplest mapping that can be used for the problem. In more general cases with complex loading paths, a morphing-like technique (e.g. [38]) can be considered.

Since the problem is fully transient and we do not assume a large database is available from the offline stage, the initial POD reduced basis cannot well represent the entire time evolution of state variables. A basis adaptation or enrichment is necessary during online computations.

In order to present the basis enrichment strategy, let us rewrite the problem (32) in the following residual form

$$\boldsymbol{\Psi}^T \mathbf{W} \mathbf{R}(\boldsymbol{\Psi}, \boldsymbol{\alpha}, \mathbf{u}, t) = 0 \tag{38}$$

where **R** is the residual vector of the energy conservation equation for a given basis Ψ , the corresponding coefficient α and flow velocity **u** at time t. It is obvious that the residual is vanishing if and only if the reduced basis Ψ spans the "exact" solution subspace. In addition, we can notice that **WR** is the error vector perpendicular to the reduced subspace span(Ψ). Therefore, **WR** should contain the information outside of span(Ψ) and can be used to enrich the reduced basis, which can be written as

$$\boldsymbol{\varPsi}^{new} = [\boldsymbol{\varPsi}, \mathbf{WR}] \tag{39}$$

It should be highlighted that this enrichment is not expensive since the residual vector \mathbf{R} only needs to be evaluated for the components in Ω_{RID} . Therefore, this enrichment can be done repetitively in a solution loop at a very low cost. Based on the solution algorithm shown in Section 2, we present here an efficient enrichment strategy including the basis mapping.

- 1. At time step t_{n+1} .
- 2. Initialization for **h**, **u** and **p**.
- 3. Mapping for reduced basis $\Psi = \Psi^0(\mathbf{X}) = \mathcal{M}(\Psi(\mathbf{X}; t_n))$.
- 4. Update Ω_{RID} and solve the hyper reduced energy equation (32) for α and update \mathbf{h} .
- 5. Solve the fluid flow problem to get correct **u** and **p**.
- 6. Update \mathcal{K} and \mathbf{Q} with \mathbf{u} and \mathbf{h} for Ω_{RID} .
- 7. Check the global energy convergence criterion: $\Psi^T \mathbf{WR}(\Psi, \alpha, \mathbf{u}, t) = 0$. If convergence, go to step 8, otherwise, return to step 4 for a new **h**.
- 8. Check the residual in Ω_{RID} : **WR** = 0. If convergence, go to next time step, otherwise, reduced basis enrichment: $\Psi = [\Psi, WR]$, and return to step 4.

It can be noticed that this method explicitly ensures the energy balance in Ω_{RID} with the converged solution. The global energy balance: $\mathbf{R}=0$ in the entire domain Ω is expected to be full-filled with an appropriate reduced basis. Furthermore, the enriched reduced basis has gappy information in $\Omega \setminus \Omega_{RID}$. Hence, this gappy reduced basis may not be optimal, although the orthogonality property remains true. A learning technique will be proposed to improve this point in Section 4.5.

4.4. Reduced integration domain adaptivity

According to the presented basis enrichment strategy, both the RID and basis would be updated frequently. In particular, the basis enrichment introduces different spatial distribution of state variables and would lead to the growth of the domain Ω_{RB} and consequently the growth of Ω_{RID} . In addition, since the melt pool region is updated in each iteration, the thermal fluid interaction domain Ω_{fl} should be updated accordingly. Hence, the RID is adaptively selected during online computations.

In general, the integration domain Ω_{RID} can grow toward the global domain Ω . This may lead to the loss of efficiency of the method and perhaps an oversized RID containing unnecessary elements or volumes. In order to avoid this problem, an adaptation boundary can be prescribed for the RID as

$$\Omega_{RID} = (\Omega_{RB} \cup \Omega_{BC} \cup \Omega_{f_l}) \cap \Omega_{MAX} \tag{40}$$

where Ω_{MAX} denotes the biggest admissible adaptation domain and should be defined a priori for a given problem. This domain is not difficult to choose since we always have some knowledge on the solution or at least the mesh information of a full order model. This domain can be simply defined as the region in which the mesh is relatively refined or the empirical region that contains the most relevant information of the solution.

4.5. Gappy reduced basis compression and reconstruction

As mentioned earlier, the enriched gappy reduced basis may not be optimal. Here we propose a learning technique to compress and reconstruct the reduced basis. The idea is to consider the solution computed by the gappy basis as a kind of gappy data and then use the gappy POD method [39] to reconstruct a new compact reduced basis.

The reduced basis learning problem can be formulated as finding an orthogonal basis Φ such that

$$\boldsymbol{\Phi} = \underset{s.t.\mathbf{Y}^T\mathbf{Y}=\mathbf{I}}{\operatorname{argmin}} \sum_{i=1}^k \|\mathbf{W}\mathcal{M}(\boldsymbol{\Psi}(\mathbf{X};t_i))\boldsymbol{\alpha}(t_i) - \mathbf{Y}\mathbf{Y}^T\mathbf{W}\mathcal{M}(\boldsymbol{\Psi}(\mathbf{X};t_i))\boldsymbol{\alpha}(t_i)\|_2^2$$
(41)

where $\Psi(\mathbf{X};t_i)$ and $\alpha(t_i)$ are respectively the enriched gappy reduced basis and its coefficient at different time steps. We assume they are known for up to step t_k . $\mathcal{M}(\Psi(\mathbf{X};t_i))$ denotes the basis mapping to current loading step. The reason behind this is the same as what is mentioned previously: the similarity of the basis exits in the region surrounding the heat source. Since the sampling indicator matrix \mathbf{W} has nonzero components in Ω_{RID} , the minimizer $\boldsymbol{\Phi}$ guarantees first its components in Ω_{RID} have the same approximation accuracy as $\boldsymbol{\Psi}$, and then uses this local information to reconstruct the remaining components. This problem can be solved with an iterative incremental procedure using standard SVD, as shown in Algorithm 1.

In general, this learning procedure is not expensive and can be done in every time step or once in several steps. From our experience, once in 10 steps is good enough for most cases. In addition, the learning procedure can only take into account several previous steps instead of all the previous solutions, e.g. the index i in (41) can start from i = k - 9 to account for previous 10 steps.

4.6. Overall offline-online algorithm

Similar to most of the POD model reduction methods, the presented hyper reduction method can be splitted into an offline-online framework, which is summarized as follows.

The offline stage of the method consists in finding an initial reduced basis which can be used to describe the spatial distribution of state variables at the very beginning of the heating. The suggested method is to run the reference full order model for a small number of time steps (e.g. 3 or 5) to get a sampling database \mathbf{h}_s and then use SVD (23)–(27) to get the initial basis. Nevertheless, this can be done by assigning an empirical or analytical one, or directly extracting from experimental data. Hence, this offline stage is not time-consuming, unlike many other model reduction methods. The detailed offline procedure is presented in Algorithm 2.

The online stage consists in solving the hyper reduced order model of the underlying multi-physics system. In the thermal fluid flow analysis, the three conservation equations (17)–(19) are solved. Again, the presented reduction strategy is applicable to all the three equations, but we only consider to reduce the thermal one for illustration. The overall online stage consisting of the presented RID adaptation and reduced basis learning is summarized in Algorithm 3.

Algorithm 1: Reduced basis learning via gappy POD

```
Input: Gappy reduced basis and coefficient: \Psi(X; t_i), \alpha(t_i), \forall i < k
      Output: New reduced basis: \Psi_{new}(\mathbf{X})
 1 Map the basis to step t_k: \Psi^*(\mathbf{X}; t_i) = \mathcal{M}(\Psi(\mathbf{X}; t_i)), \forall i < k
 2 Reconstruction of \Delta \mathbf{h} = \left[ \boldsymbol{\Psi}^*(\mathbf{X}; t_1) \boldsymbol{\alpha}(t_1), \dots, \boldsymbol{\Psi}^*(\mathbf{X}; t_k) \boldsymbol{\alpha}(t_k) \right]
 3 for m = 1, ..., k do
              for i = 0, \ldots, i_{\text{max}} do
 4
                      Compute the first m modes of \Delta \mathbf{h} by thin SVD: \boldsymbol{\Phi}_m, \boldsymbol{\Sigma}_m, \mathbf{V}_m
                                                                                                                                                                                                                   // Eq. (23)
 5
                      Compute an estimate with the m modes: \Delta \tilde{\mathbf{h}}^{i+1} = \boldsymbol{\Phi}_m \boldsymbol{\Sigma}_m \mathbf{V}_m^T
 6
                      Update the reference: \Delta \mathbf{h}(\mathbf{X}) = \Delta \tilde{\mathbf{h}}^{i+1}(\mathbf{X}), \forall \mathbf{X} \in \Omega \setminus \Omega_{RID}
 7
                      /* Check the mode convergence:
                                                                                                                                                                                                                                          */
                      \begin{array}{c|c} \text{if } \underline{\|\Delta\tilde{\mathbf{h}}^{i+1} - \Delta\tilde{\mathbf{h}}^i\| \leq \epsilon_i} \text{ then} \\ | & \Delta\mathbf{h}^m = \Delta\mathbf{h} \end{array}
 8
 9
                              End the Loop i
10
                      else
11
                       (\cdot)^i \leftarrow (\cdot)^{i+1}
12
              /* Check the basis convergence:
                                                                                                                                                                                                                                          */
             if \|\Delta \mathbf{h}^m - \Delta \mathbf{h}^{m-1}\| \le \epsilon_m then
\Psi_{new}^{(j)} = \sqrt{\sigma^{(j)}} \Phi_m^{(j)}, \forall j \le m
End the Loop m
13
14
15
16 Return \boldsymbol{\varPsi}_{new} = [\boldsymbol{\varPsi}_{new}^{(1)}, \ldots, \boldsymbol{\varPsi}_{new}^{(m)}]
```

Algorithm 2: Offline stage of the adaptive hyper reduction method

```
Input: Small simulated database via the full order model: \mathbf{h}_s = [\mathbf{h}(t_1), \dots, \mathbf{h}(t_s)]
Output: Initial reduced basis for hyper reduction: \Psi_0

1 Compute the reference \Delta \mathbf{h}_s = \mathbf{h}_s - \mathbf{h}(t_0)

2 Compute the POD basis of \Delta \mathbf{h}_s by thin SVD: \Phi_m with m = s

3 Compute the amplified basis \Psi_0^{(j)} = \sqrt{\sigma^{(j)}} \Phi_m^{(j)}, \forall j \leq m

4 Return \Psi_0 = [\Psi_0^{(1)}, \dots, \Psi_0^{(m)}]
```

5. Application to additive manufacturing

5.1. Model description

The proposed method is applied to model the thermal fluid interaction in a selective laser melting process with bare plate scans. As a first attempt, the powder is not considered and a relatively simple geometry is considered with a locally refined grid (see e.g Fig. 1). The mesh is refined for the expected melt pool and its surrounding region and the refined region is traveling with the moving heat source. Following an exponential law, the mesh size increases when away from the refined region. A straightforward advantage of this meshing strategy is that the basis mapping Eq. (37) from one step to another is naturally performed when updating the mesh, without explicit interpolation. The convection and radiation boundary conditions are prescribed for all the exposed surfaces. The fluid flow is driven by the buoyancy force and the Marangoni force on the top of melt pool, as presented in Section 2. The material properties are considered temperature-dependant. These properties as well as the parameters used in boundary conditions and loading are illustrated in Table 1.

In order to demonstrate the capability of the method, two 3D test-cases are considered: single-track and multi-track models. They are designed with the same boundary conditions and material set-up (as described previously) but with different geometry dimensions and mesh sizes. The geometry and mesh information is described as follows.

Algorithm 3: Online stage of the adaptive hyper reduction method

```
Input: Initial reduced basis \Psi_0 and state variables h, u and p
    Output: Space-time solution of the problem: h(X, t), u(X, t) and p(X, t)
 1 Initialization of reduced basis: \Psi(X; t_0) = \Psi_0
 2 for t_k = t_1, ..., t_{max} do
         Mapping for reduced basis \Psi(\mathbf{X}) = \mathcal{M}(\Psi(\mathbf{X}; t_{k-1}))
 3
         Update \Omega_{RB}, \Omega_{BC}, \Omega_{f_l}
 4
         Update \Omega_{RID} and indicator matrix W
                                                                                                                                                 // Eq. (40)
 5
         for i = 1, ..., i_{max} do
 6
 7
               Update WK and WQ
               Solve the hyper reduced energy equation for \alpha
                                                                                                                                                 // Eq. (32)
 8
               Reconstruction of \mathbf{h} = \bar{\mathbf{h}} + \boldsymbol{\Psi}\boldsymbol{\alpha}
               /* Solve other physics quantities
               Solve the fluid flow problem to get correct u and p for fixed h
                                                                                                                                                    // SIMPLE
10
               /* Check the global energy convergence
               if \| \boldsymbol{\Psi}^T \mathbf{W} \mathbf{R}^i (\boldsymbol{\Psi}, \boldsymbol{\alpha}, \mathbf{u}, t) \| \leq \epsilon_e \| \boldsymbol{\Psi}^T \mathbf{W} \mathbf{R}^0 \| then
11
                    /* Check the residual in \Omega_{RID}
                    if \|\mathbf{W}\mathbf{R}^i\| \leq \epsilon_b \|\mathbf{W}\mathbf{R}^0\| then
12
                          \mathbf{h}(\mathbf{X}, t_k) = \mathbf{h}
13
                          \mathbf{u}(\mathbf{X}, t_k) = \mathbf{u}
14
                          \mathbf{p}(\mathbf{X}, t_k) = \mathbf{p}
15
                           \Psi(\mathbf{X}, t_k) = \Psi
16
                          \alpha(t_k) = \alpha
17
                          End the loop i
18
                    else
19
                          Reduced basis enrichment: \Psi = [\Psi, WR]
20
               Update the melt pool region \Omega_{f_l} but not \Omega_{RB}
21
               Update \Omega_{RID} and W
                                                                                                                                                 // Eq. (40)
22
         if t_k = specific steps, e.g. [t_{10}, t_{20}, t_{30}, \cdots] then
23
            Gappy reduced basis reconstruction \Psi
                                                                                                                                           // Algorithm 1
24
         Return \mathbf{h}(\mathbf{X}, t_k), \mathbf{u}(\mathbf{X}, t_k) and \mathbf{p}(\mathbf{X}, t_k)
25
```

- Single-track model. The lengths in the three directions (x, y, z) are respectively: 5.4, 1.25, 0.6 ($\times 10^{-3}$ m). The number of elements in three directions is respectively: 120, 50, 30. This results in a mesh size of 180000. The moving heat source velocity in the *x*-direction is 0.8 m.s⁻¹. The track length is about 3.6 $\times 10^{-3}$ m.
- Multi-track model. The lengths in the three directions (x, y, z) are respectively: 2.3, 1.4, 0.6 $(\times 10^{-3} \text{ m})$. The number of elements in three directions is respectively: 150, 83, 30. This results in a mesh size of 373500. The moving heat source velocity in the *x*-direction is 1.2 $m.s^{-1}$. Three tracks will be performed with a deviation of 0.1×10^{-3} m in the *y*-direction. Each single track length is about 0.84×10^{-3} m.

Since the melt pool region is expected to be very small compared to the whole domain, the main computational cost for such thermal fluid coupled problems is devoted to the thermal part. Hence, only the thermal energy equation will be reduced in the test-cases. The fluid problem is solved in a standard way. For comparison purposes, the solutions provided by full order models (17)–(19) based on the same numerical set-up will serve as a reference.

Although the track length in the test-cases is still small compared to real experiments, the main features of the problem is captured, especially the highly transient and nonlinear aspects. The application to a larger model is straightforward, since the temperature field will reach a steady state in a long term set-up. In that case, the reduced basis can be repetitively used without adaptation.



Fig. 1. Mesh for a single-track model at two different time instants. In particular, the mesh is relatively refined in the back side of loading, compared to the front side. Red box shows an example for the choice of maximal RID adaptation domain Ω_{MAX} .

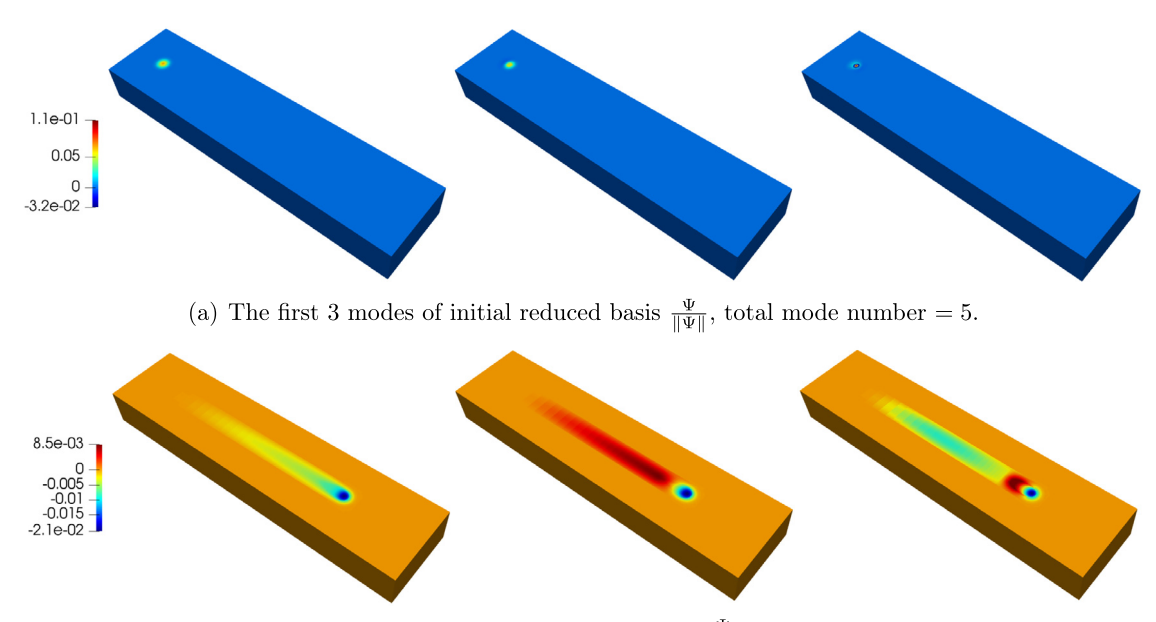
Table 1 Process parameters and material properties of IN625 [9,5].

Name	Properties	Value	
Solid density	ρ_s (kg.m ⁻³)	8440	
Liquid density	$\rho_l \text{ (kg.m}^{-3}\text{)}$	7640	
Solidus temperature	T_s (K)	1523	
Liquidus temperature	T_l (K)	1623	
Solid specific capacity	C_{ps} (J.kg ⁻¹ .K ⁻¹)	$0.2441 \times T + 338.39$	
Liquid specific capacity	C_{pl} (J.kg ⁻¹ .K ⁻¹)	709.25	
Solid thermal conductivity	k_s (W.m ⁻¹ .K ⁻¹)	$0.0163 \times T + 4.5847$	
Liquid thermal conductivity	$k_l (W.m^{-1}.K^{-1})$	30.078	
Latent heat of fusion	ΔH (J.kg ⁻¹ .K ⁻¹)	290×10^{3}	
Viscosity	μ (Pa.s)	7×10^{-3}	
Thermal expansion coefficient	β (K ⁻¹)	5×10^{-5}	
Marangoni coefficient	$\frac{d\gamma}{dT}$ (N.m ⁻¹ .K ⁻¹)	-4×10^{-4}	
Emissivity	ε	0.4	
Stefan-Boltzmann constant	$\sigma_s \ ({\rm W.m^{-2}.K^{-4}})$	5.67×10^{-8}	
Convection coefficient	$h_c \text{ (W.m}^{-2}.\text{K}^{-1})$	10	
Initial temperature	T_0 (K)	295	
Loading intensity factor	ϵ	0.25	
Power	Q (W)	195	
Absorptivity	η	0.43	
Radius	r_b (m)	3.825×10^{-5}	

5.2. Single-track simulation

In this single-track simulation, the time discretization is as follows: $\Delta t = 1 \times 10^{-6}$ s, 5×10^{-6} s, 1×10^{-5} s for the first three time steps, then $\Delta t = 1 \times 10^{-5}$ s for the rest. At the offline stage, the solutions are computed with full order model (FOM) for the first five steps. This database provides the initial reduced basis and the initial RID for the hyper reduced order model (HROM). The selection thresholds for Ω_{RB} (33) and Ω_{BC} (34) are chosen as $c_{RB} = 0.01$ and $c_{BC} = 0.1$. The maximal adaptation domain Ω_{MAX} is chosen as the region with relatively finer mesh: the surrounding region of loading and the back side, as shown in the red box in Fig. 1.

During the online computations, the reduced basis and RID are adaptively updated with the proposed strategy. Fig. 2 illustrates the initial reduced basis and the final one. It is shown that the final basis can be significantly different from the initial one. This clearly shows the challenges associated with standard model reduction methods: a large number of necessary modes, i.e. the lack of reducibility of the problem. Fortunately, the proposed strategy allows to efficiently learn the basis evolution while keeping a relatively small size of the basis. Fig. 3 depicts the basis size evolution during the online computations. The maximal size is less than 35 in this example. This is, in particular, owed to the gappy basis compression and reconstruction. The final basis contains only 12 modes when



(b) The first 3 modes of final updated reduced basis $\frac{\Psi}{\|\Psi\|}$, total mode number = 12.

Fig. 2. Evolution of the reduced basis in HROM.

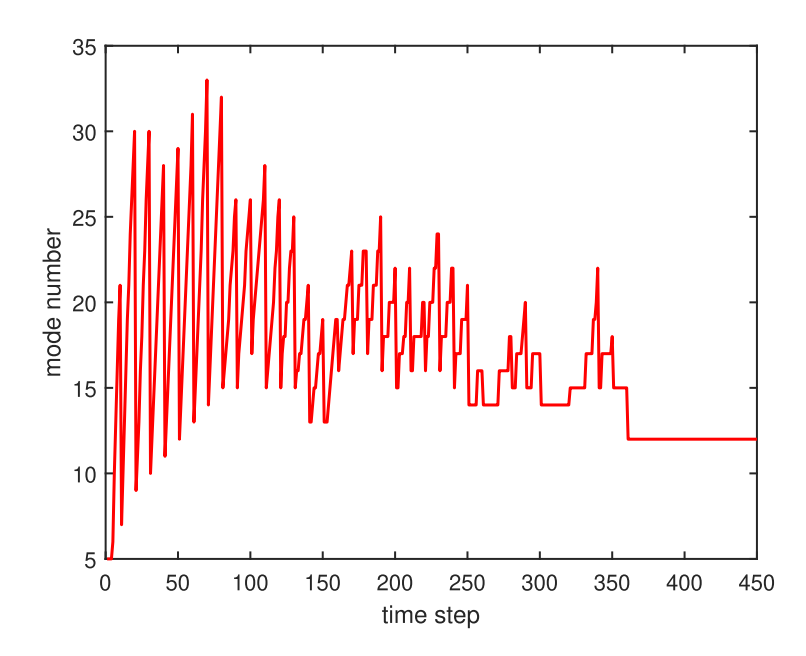


Fig. 3. Evolution of the size of reduced basis in HROM for the single-track problem. The decrease of modes corresponds to the basis compression via the proposed technique.

the temperature field reaches the so-called steady-state. The evolution of RID with the local temperature field is shown in Fig. 4. This evolution is obviously related to the evolution of reduced basis and it dominates the online computational cost. It can be expected that the RID remains unchanged once the temperature enters into a relatively stable regime.

The full field solutions reconstructed with the reduced basis and the computed coefficients are illustrated in Fig. 5(b)(d). Compared to the reference FOM solutions, both thermal and fluid solutions show a very good

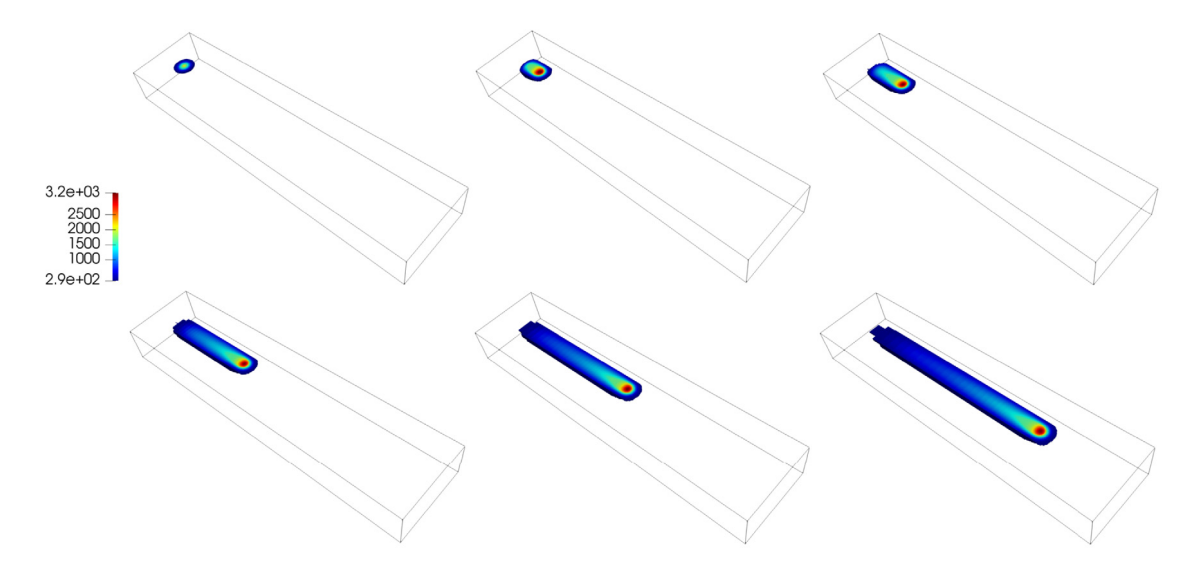


Fig. 4. Evolution of the reduced integration domain in HROM with local temperature field T(K).

agreement. The local temperature difference between the HROM and FOM is depicted in Fig. 6. We can observe that the small difference comes from the back of the heat source region and mostly the region undergoing a cooling stage. This point may be improved by modifying the adaptation criteria used in the algorithm and will be studied in our future development.

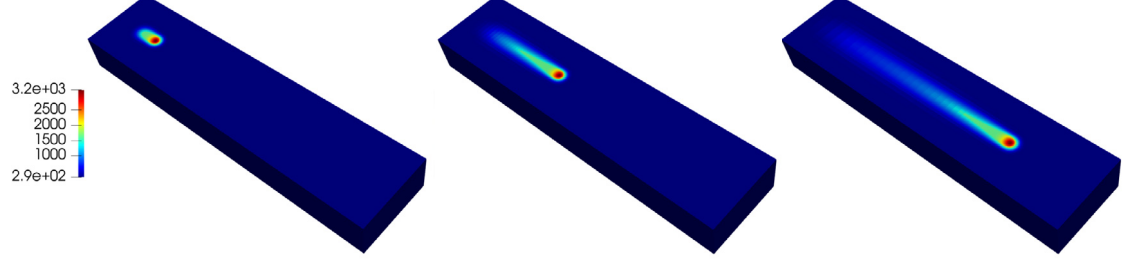
Fig. 7 compares the melt pool shapes obtained with the HROM and FOM. We can notice that the computed melt pool size in the cross section has a very good accuracy. This is reasonable and confirms that the temperature field around the melt pool is well approximated. This measure is usually used as key characteristics in additive manufacturing processes for model calibration.

In order to illustrate the influence of the RID selection threshold c_{RB} . The comparison for three different values is performed (see Fig. 8). A HROM solution without the gappy basis compression and reconstruction is depicted in Fig. 8(d) for comparison. It is shown that a smaller threshold leads to a larger RID (especially in the back side of heat source) and consequently a better approximation for the region undergoing cooling stage. A convergence can be found by decreasing the threshold. Table 2 summarizes some important quantities obtained by different models. This confirms the convergence of the proposed HROM to the FOM when decreasing the RID selection threshold. All three hyper reduced models agree well with FOM in terms of the key measures. Interestingly, the size of final reduced basis decreases as well with the threshold. This may be related to the smoothness of the solution. A smaller threshold seems to provide a better smoothness for the region in the back of heat source. Nevertheless, any of the three HROM solutions is much better than the one depicted in Fig. 8(d), in terms of smoothness or regularity. This confirms the important role played by the proposed gappy basis learning strategy.

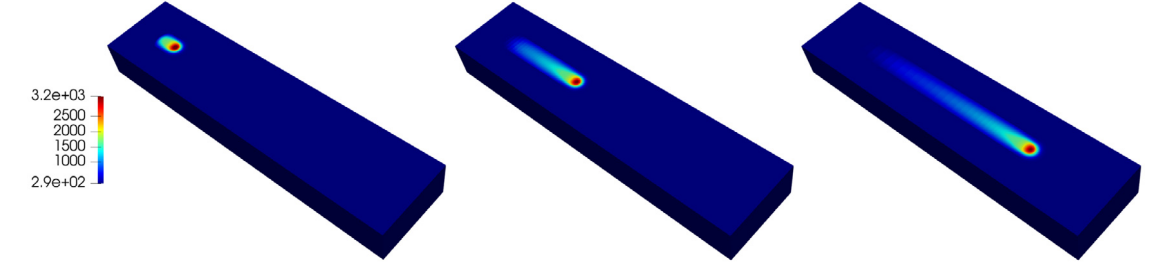
The computational cost for different models is summarized in Table 3. First, it confirms that the computation cost of a FOM is mainly devoted to the thermal problem in this thermal fluid analysis. Hence, reducing the thermal cost seems more crucial for speeding up the simulations. Indeed, applying the proposed hyper reduction method to the thermal part has enabled a significant speed-up.

For a better visualization, we illustrate the accuracy of the HROM solutions as a function of the speed-up in Fig. 9. It is shown that a higher speed-up would lead to a slightly degraded accuracy. In general cases, a balance should be made between them.

Remark that in this example, the mesh size is still relatively coarse, compared to a realistic model in additive manufacturing. A higher speed-up can be expected when dealing with a larger structure or a more complex geometry which usually requires a larger mesh size.



(a) Reference FOM temperature T(K), from left to right, $t_{50}: 4.86 \times 10^{-4} s$, $t_{200}: 2 \times 10^{-3} s$, $t_{450}: 4.5 \times 10^{-3} s$.



(b) HROM temperature T(K), from left to right, $t_{50}: 4.86 \times 10^{-4}s$, $t_{200}: 2 \times 10^{-3}s$, $t_{450}: 4.5 \times 10^{-3}s$.



(c) Reference FOM flow velocity $\|\mathbf{u}\|(m.s^{-1})$, from left to right, $t_{50}:4.86\times10^{-4}s,\ t_{200}:2\times10^{-3}s,\ t_{450}:4.5\times10^{-3}s.$



(d) HROM flow velocity $\|\mathbf{u}\|(m.s^{-1})$, from left to right, $t_{50}: 4.86 \times 10^{-4}s$, $t_{200}: 2 \times 10^{-3}s$, $t_{450}: 4.5 \times 10^{-3}s$.

Fig. 5. Evolution of the reconstructed state variables in full domain for the adaptive hyper reduced order model with comparison to the reference full order model.

5.3. Multi-track simulation

The reduced order modeling of the multi-track problem is much more challenging, since the interactions of different tracks need to be captured and this can lead to significant changes in the reduced basis. Hence, the reducibility of such problem is questionable and very few works have considered this challenging problem for reduced order modeling.

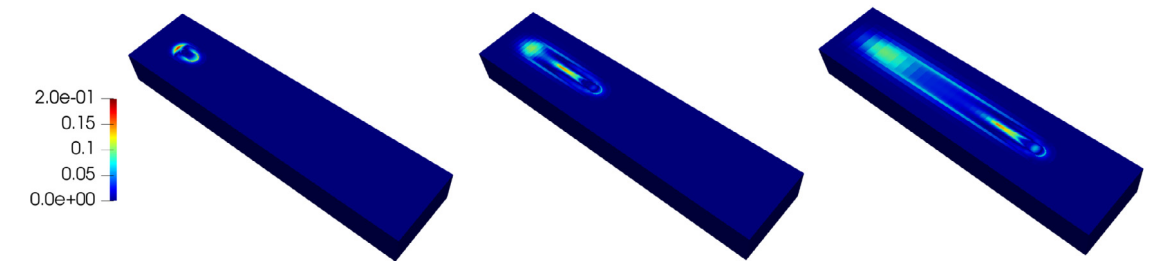


Fig. 6. Local temperature difference between the HROM and FOM: $\frac{|T-T_{\text{FOM}}|}{\|T_{\text{FOM}}\|_{\infty}}$ in different time steps, from left to right, $t_{50}:4.86\times10^{-4}$ s, $t_{200}:2\times10^{-3}$ s, $t_{450}:4.5\times10^{-3}$ s.

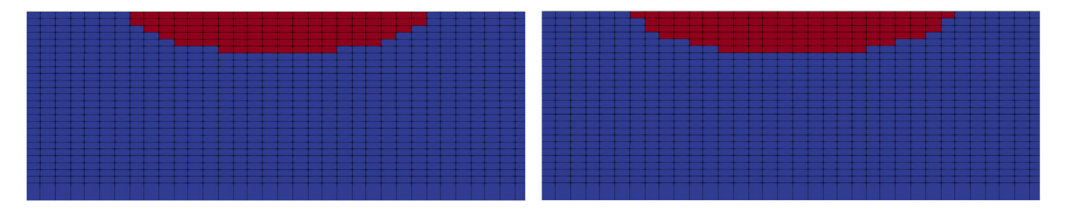


Fig. 7. Melt pool shape (red) comparison. Cross section, Left: FOM reference, Right: HROM solution.

 Table 2

 Solution quality assessment for the single-track simulation.

Model	c_{RB}	Modes	Final RID	Err(T)	Peak $T(K)$	Width (μm)	Depth (µm)
FOM	_	_	_	_	3140	175	52.5
HROM	0.05	22	59621	16.3%	3204	192.5	61.2
HROM	0.03	12	79188	12.3%	3103	192.5	52.5
HROM	0.01	12	89634	11%	3146	192.5	52.5

Remark: Width and Depth are the computed melt pool size. $\operatorname{Err}(T) = \frac{\|T - T_{\text{FOM}}\|_{L^2(\Omega \times \Omega_t)}}{\|T_{\text{FOM}}\|_{L^2(\Omega \times \Omega_t)}}$, where Ω_t stands for the time domain of solution.

 Table 3

 Computational cost for the single-track simulation.

Model	c_{RB}	Offline	Thermal online	Fluid online	Total online	Speed-up
FOM	-	-	137 h	18.5 h	155.5 h	_
HROM	0.05	1.2 h	20 h	23 h	43 h	3.6
HROM	0.03	1.2 h	28 h	18.5 h	46.5 h	3.3
HROM	0.01	1.2 h	33.4 h	19 h	52.4 h	2.97

In this work, we attempt to attack this problem within the proposed HROM framework. The scan path for the multi-track model is illustrated in Fig. 10. As previously mentioned, the mesh is locally refined around the melt pool and the refined region is traveling along the loading path. In particular, we consider that the work-piece will be cooling for 2×10^{-4} s at the end of each track, by removing the heat source. A constant time increment, 1×10^{-5} s, is used during the entire computations. Similar to the single-track problem, the solutions of first 3 time steps can be computed offline using the full order model to initialize the reduced basis. However, we can expect that the appropriate reduced basis should differ significantly from one track to another. Therefore, we propose to re-initialize the reduced basis at the beginning of each track. Furthermore, we consider that the reference initial field $\bar{\mathbf{h}}(\mathbf{X})$ is changing to the final solution of the previous track when starting a new one. The re-initialization requires online full order computations for several time steps. Our experience showed that this is not expensive, compared to the total cost of the multi-track simulation.

Figs. 11–14 illustrate the HROM results. They show a very good agreement to the reference FOM solution. The interaction between different tracks is well captured. This HROM solution is obtained with the coefficient

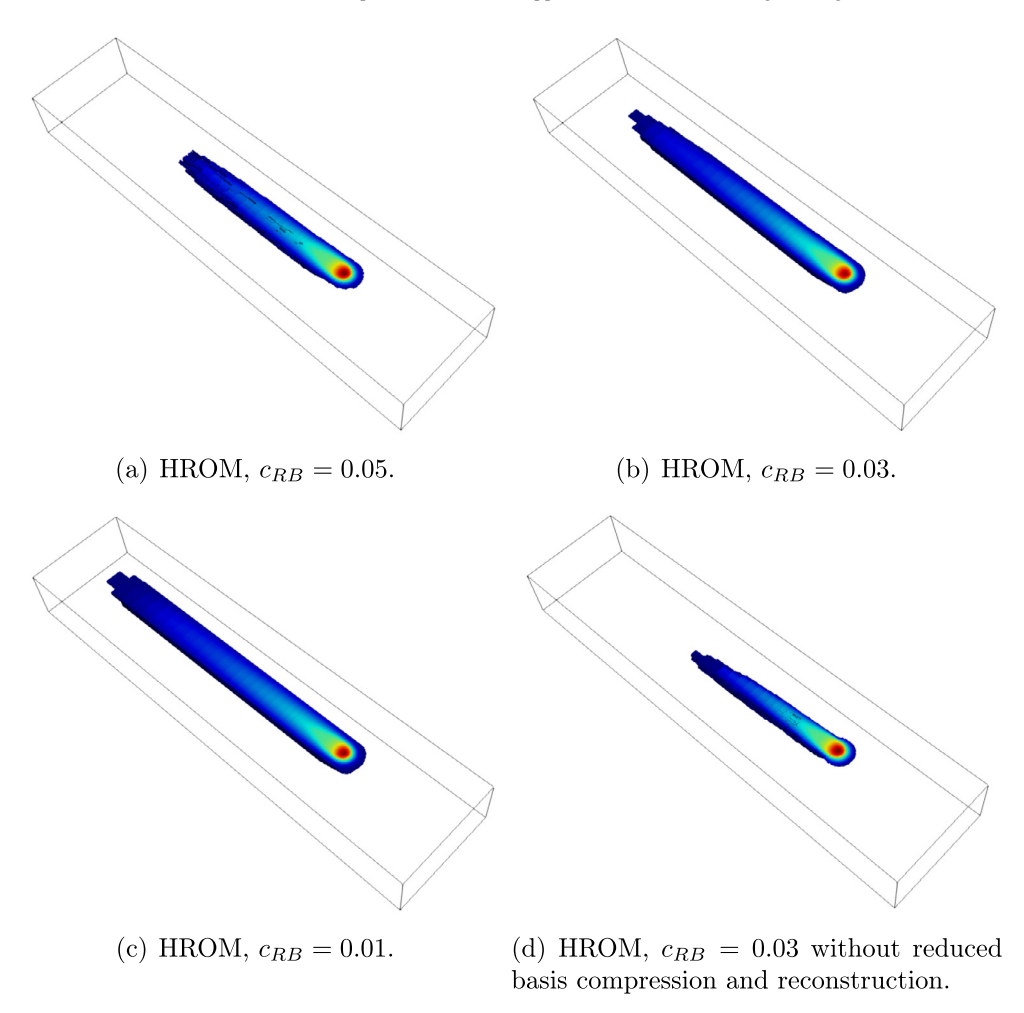


Fig. 8. Final RID for different selection thresholds $c_{RB} = 0.01, 0.03, 0.05$ and with comparison to a solution without online reduced basis compression and reconstruction.

 $c_{RB} = 0.01$. As shown in Table 4, the computed temperature field has an average error about 10%. This error can be reduced by further decreasing the coefficient c_{RB} . Furthermore, The computed melt pool size stays close to that of FOM. This confirms that the difference in the temperature fields mainly come from the region outside the melt pool region. We can observe that the temperature interaction between different tracks leads to the increase of melt pool size. As expected, the reduced basis changes significantly in different tracks for capturing the previous heating effect and consequently the RID for the second and third tracks have to be larger than the first one. This is shown in Figs. 15 and 16. We can expect that the reduced basis and integration domain will become stable when a steady state regime is reached. Again, Fig. 17 shows the capability of the gappy basis compression technique, which allows to limit the basis size below 60 over the entire time range. The computational cost for the HROM is summarized in Table 5. Significant time saving is obtained with the proposed HROM. Due to the extensive adaptation of reduced basis, the online cost for the fluid flow problem is increased compared to the FOM. This cost remains at a reasonable level, compared to the total time cost.

5.4. Discussion on computational efficiency

In our work, all the computations are performed in MATLAB with a standard computer and without parallelization. Hence, the computational cost of each model is relatively high. Although a locally refined mesh is used, the

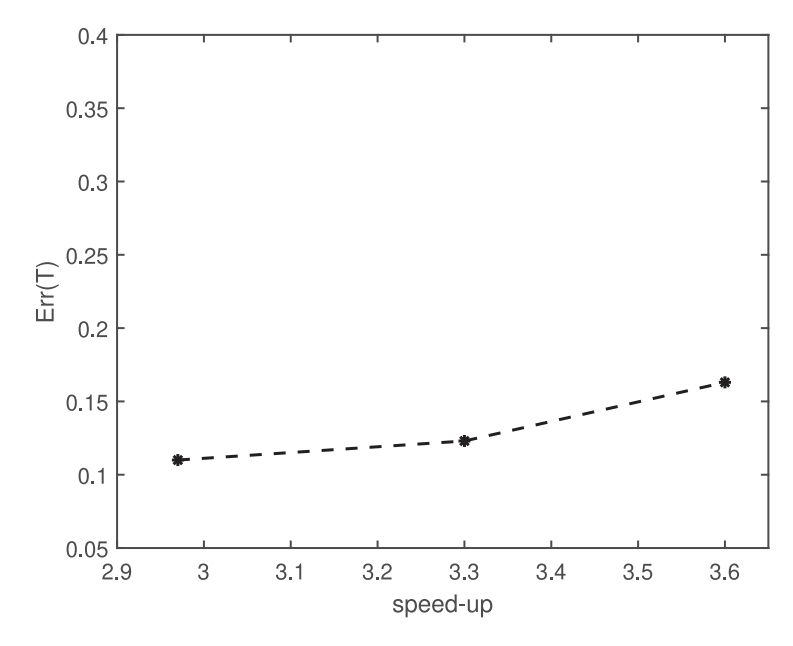


Fig. 9. Accuracy versus speed-up for the single-track simulation.

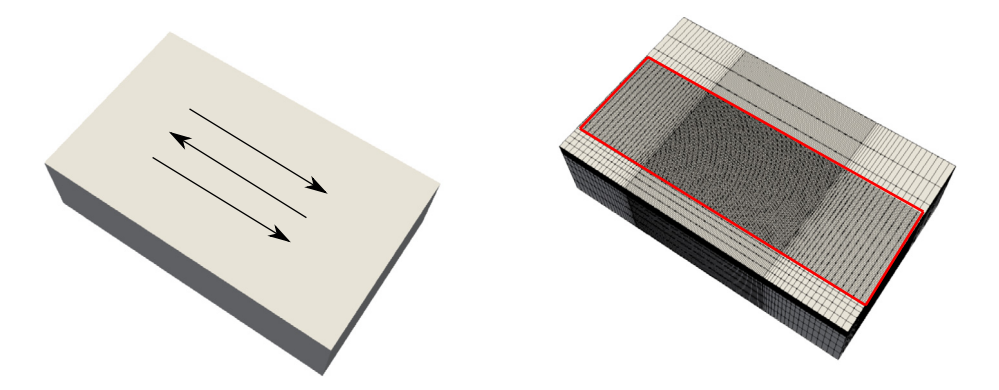


Fig. 10. Scan path (left) and mesh (right) of the multi-track model. Red box shows the boundaries of the maximal RID Ω_{MAX} .

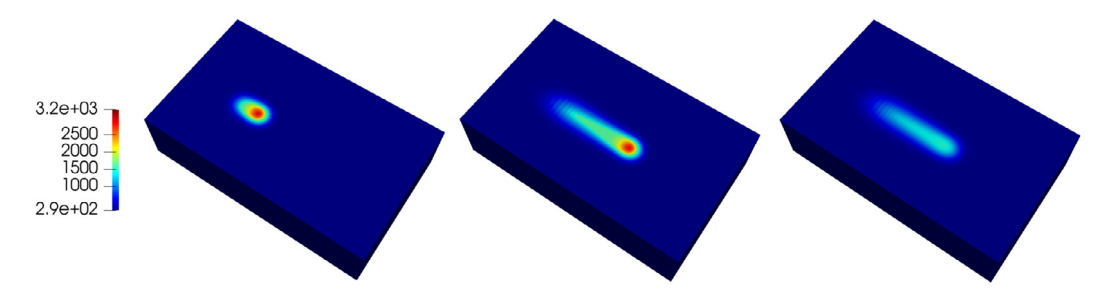
 Table 4

 Solution quality assessment for the multi-track simulation.

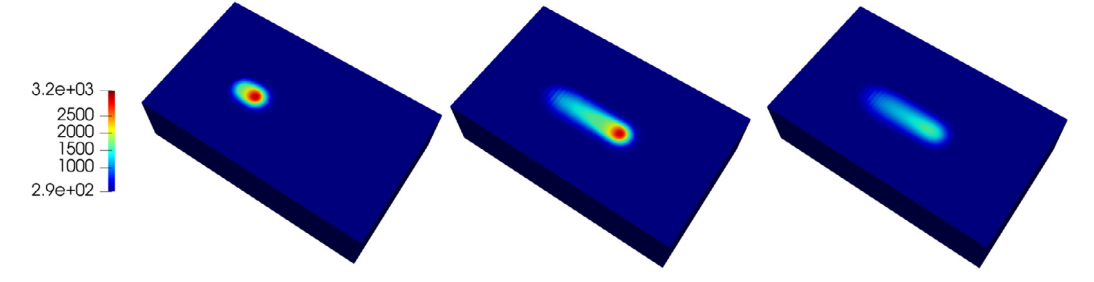
Model	c_{RB}	Err(T)	W-1 (μm)	W-2	W-3	D-1 (μm)	D-2	D-3
FOM	-	-	150	170	170	20	24	24
HROM	0.01	9.9%	170	170	170	20	24	24
HROM	0.001	7.5%	170	170	170	20	24	24

Remark: W-i and D-i stand for the maximum width and depth of the ith track. $\mathrm{Err}(T) = \frac{\|T - T_{\mathrm{FOM}}\|_{L^2(\Omega \times \Omega_t)}}{\|T_{\mathrm{FOM}}\|_{L^2(\Omega \times \Omega_t)}}$, where Ω_t stands for the time domain of solution.

cost of FOM remains important and is mostly devoted to the stiffness matrix updating and inversion in different time steps and iteration loops. Obviously, more advanced adaptive meshing techniques can be used to improve the efficiency of FOM. However, this may be difficult when dealing with large and complex geometries. The proposed hyper reduction method can be viewed as an alternative, since the effective computation domain (i.e. RID) can remain very small regardless of the mesh size. This implies that a uniformly refined mesh can be used with the

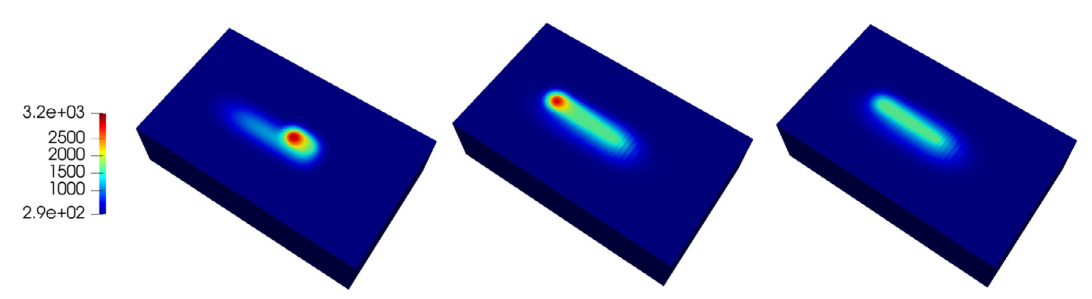


(a) Reference FOM T(K), from left to right, $t_{20}: 2 \times 10^{-4}s$, $t_{70}: 7 \times 10^{-4}s$, $t_{90}: 9 \times 10^{-4}s$.

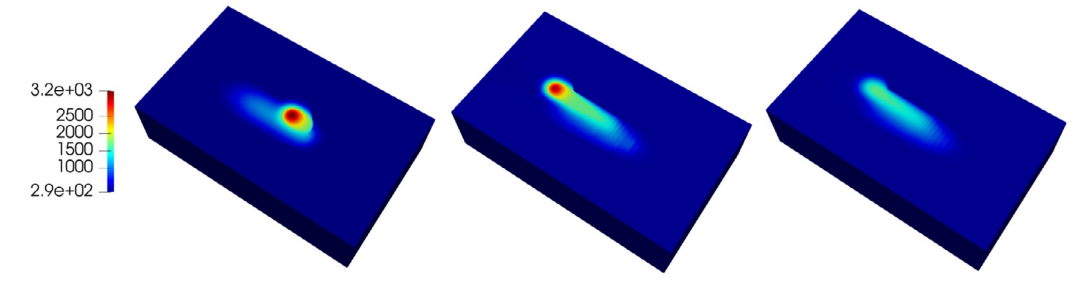


(b) HROM T(K), from left to right, $t_{20}: 2 \times 10^{-4}s$, $t_{70}: 7 \times 10^{-4}s$, $t_{90}: 9 \times 10^{-4}s$.

Fig. 11. Temperature profile snapshots in the first track.

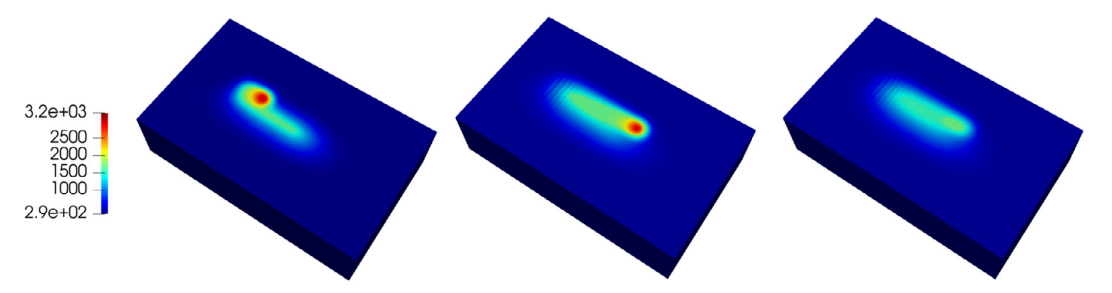


(a) Reference FOM T(K), from left to right, $t_{110}: 1.1 \times 10^{-3}s, \ t_{160}: 1.6 \times 10^{-3}s, \ t_{180}: 1.8 \times 10^{-3}s$.

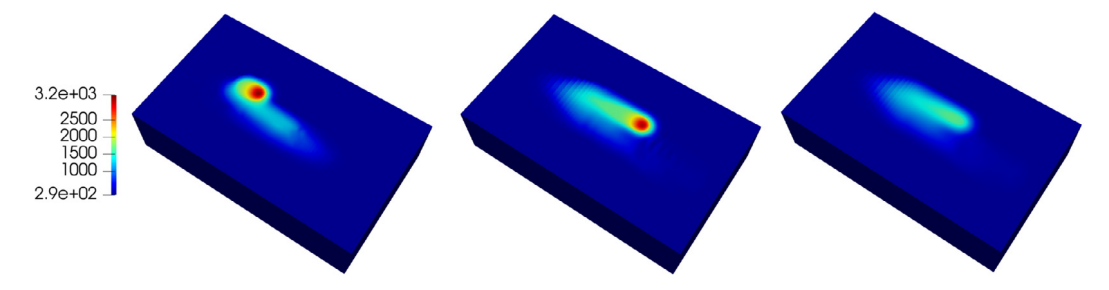


(b) HROM T(K), from left to right, $t_{110}: 1.1 \times 10^{-3}s$, $t_{160}: 1.6 \times 10^{-3}s$, $t_{180}: 1.8 \times 10^{-3}s$.

Fig. 12. Temperature profile snapshots in the second track.



(a) Reference FOM T(K), from left to right, $t_{200}: 2\times 10^{-3}s,\ t_{250}: 2.5\times 10^{-3}s,\ t_{270}: 2.7\times 10^{-3}s.$

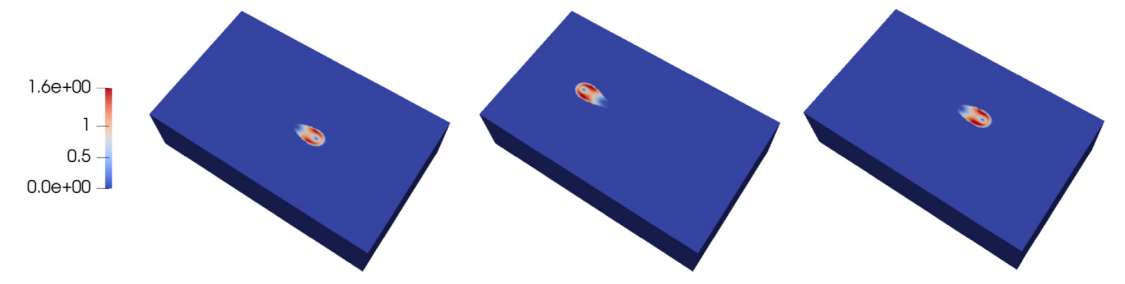


(b) HROM T(K), from left to right, $t_{200}: 2 \times 10^{-3}s, \, t_{250}: 2.5 \times 10^{-3}s, \, t_{270}: 2.7 \times 10^{-3}s.$

Fig. 13. Temperature profile snapshots in the third track.



(a) Reference FOM $\|\mathbf{u}\|(m.s^{-1})$, from left to right, $t_{70}: 7 \times 10^{-4}s$, $t_{160}: 1.6 \times 10^{-3}s$, $t_{250}: 2.5 \times 10^{-3}s$.



(b) HROM $\|\mathbf{u}\|(m.s^{-1})$, from left to right, $t_{70}: 7 \times 10^{-4}s$, $t_{160}: 1.6 \times 10^{-3}s$, $t_{250}: 2.5 \times 10^{-3}s$.

Fig. 14. Flow velocity magnitude in the multi-track model.

hyper reduction method at an affordable cost, even for a large structure. Therefore, the cumbersome meshing and re-meshing procedure can be avoided.

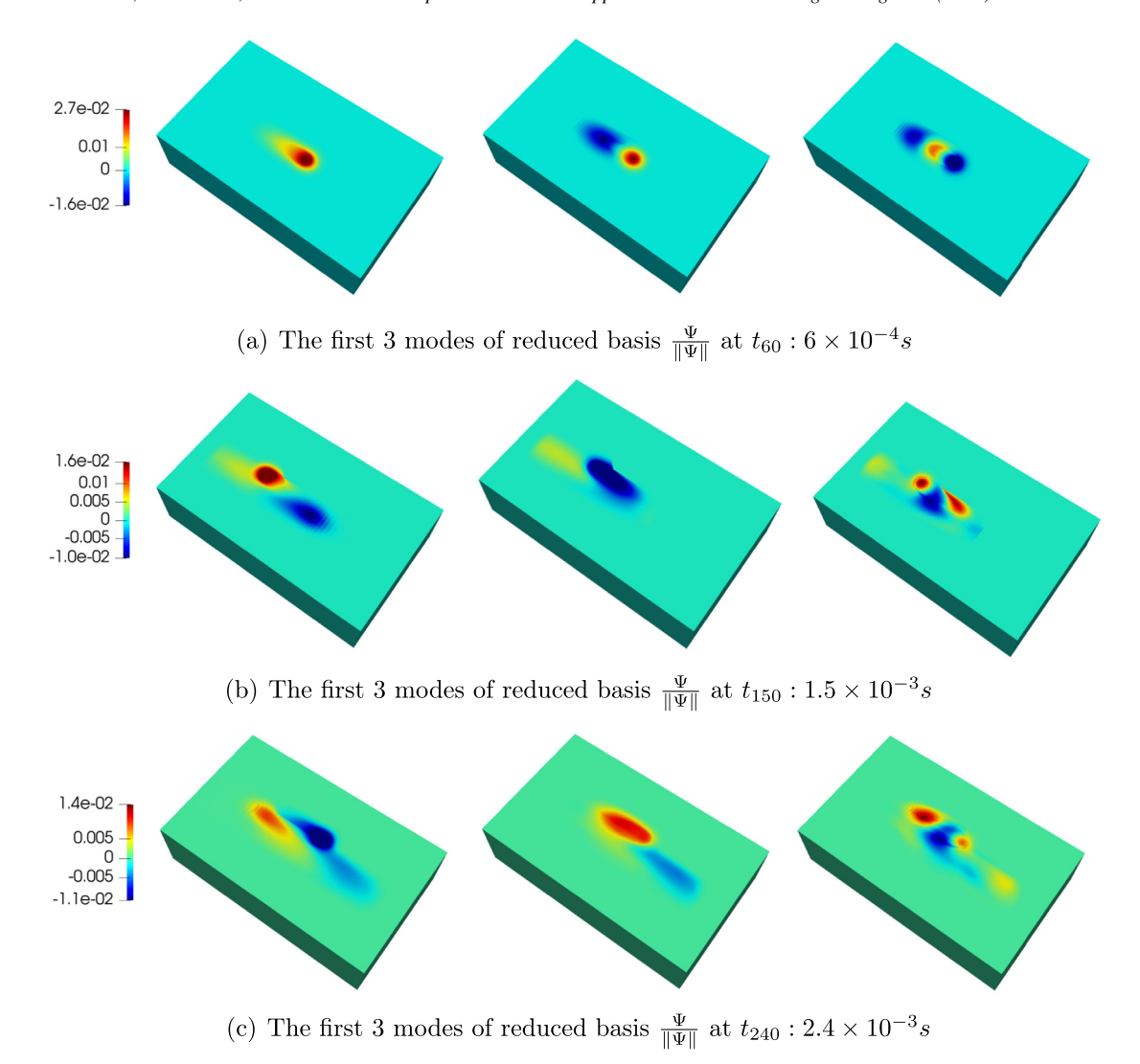


Fig. 15. Evolution of reduced basis in the multi-track model. The basis for the second (b) and third (c) track is altered by the influence from previous tracks.

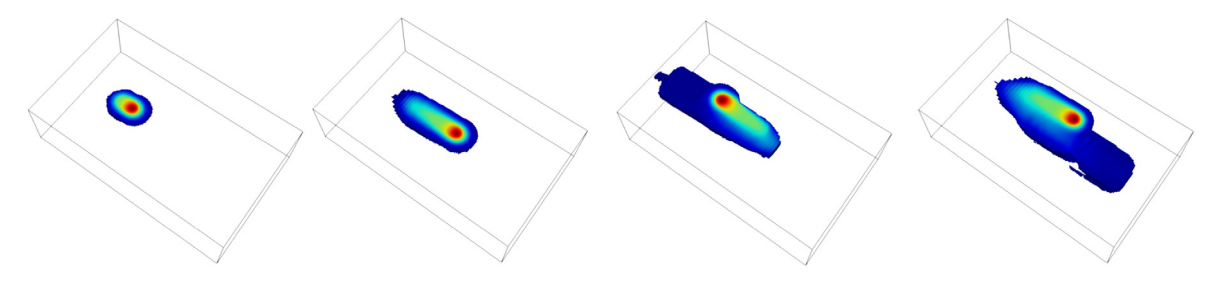


Fig. 16. Evolution of the reduced integration domain with local temperature field in the multi-track model, from left to right, $t_{20}: 2 \times 10^{-4} \text{ s}$, $t_{60}: 6 \times 10^{-4} \text{ s}$, $t_{150}: 1.5 \times 10^{-3} \text{ s}$, $t_{240}: 2.4 \times 10^{-3} \text{ s}$.

The speed-up obtained in the presented examples is around 3. A higher factor can be expected when considering a large mesh size (especially uniformly refined mesh) or smaller time steps.

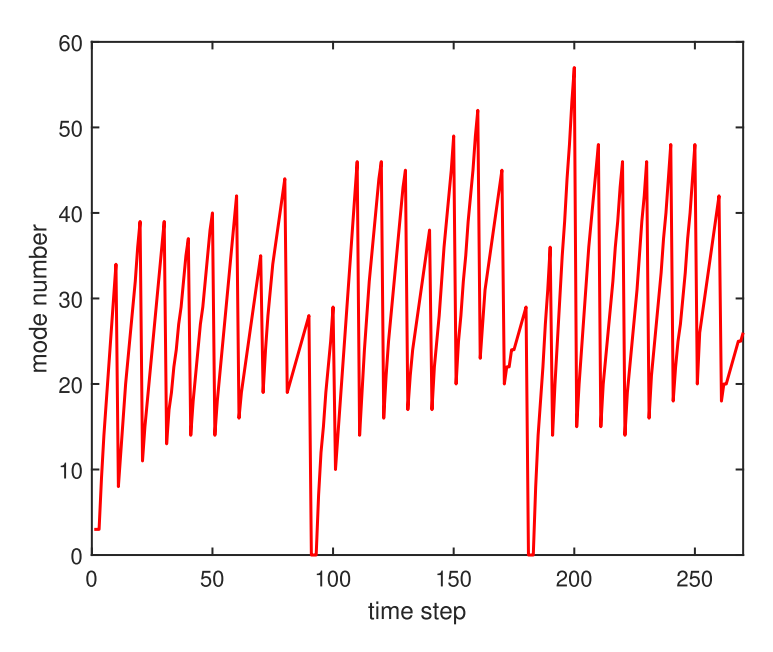


Fig. 17. Evolution of the size of reduced basis in HROM for the multi-track problem. Steps 91 and 181 correspond to the re-initiation steps.

 Table 5

 Computational cost for the multi-track simulation.

Model	c_{RB}	Offline	Thermal online	Fluid online	Total online	Speed-up
FOM	_	_	305.9 h	13.4 h	319.3 h	_
HROM	0.01	3.1 h	59.8 h	31.3 h	91.1 h	3.5
HROM	0.001	3.1 h	103.2 h	30.5 h	133.7 h	2.4

6. Conclusion

A novel adaptive hyper reduction method has been proposed. This method is based on an online adaptation strategy for both reduced basis and reduced integration domain. The efficiency of basis adaptation is ensured by a local residual enrichment strategy following a basis mapping. Then, the quality of the enriched basis is ensured by a proposed gappy basis learning technique.

The proposed hyper reduction method has been successfully applied to a highly nonlinear and transient thermal fluid analysis for additive manufacturing. In particular, the challenging multi-track problem is also considered in this work. It is shown that both single-track and multi-track problems can be solved with a unified hyper reduction framework. A significant speed-up is obtained for both problems.

Future development can study the influence of different selection criteria (e.g. higher order derivatives) for the reduced integration domain or consider a more advanced morphing technique [38] for the basis mapping. Another direction is to extend the proposed method to account for other physics in additive manufacturing, e.g. the macroscopic thermo-mechanical prediction. In addition, this method can be used as a data or snapshot generator for other data-driven non-intrusive model reduction techniques (e.g. [28,29]) or artificial neural network based approaches (e.g. [40]), for real time simulations. Concerning the modeling aspect, advanced techniques like Cut finite element methods [41] could be considered for capturing complex geometry (or phase) changes during the manufacturing process.

Declaration of competing interest

The authors declare that they have no known competing financial interests or personal relationships that could have appeared to influence the work reported in this paper.

Acknowledgments

The authors would like to acknowledge the support of the National Science Foundation under Grant No. CMMI-1934367. Kevontrez K. Jones would like to thank the Murphy Fellowship provided by Northwestern University. Ye Lu would like to thank Zhiyong Li for helpful discussion.

References

- [1] J. Smith, W. Xiong, W. Yan, S. Lin, P. Cheng, O.L. Kafka, G.J. Wagner, J. Cao, W.K. Liu, Linking process, structure, property, and performance for metal-based additive manufacturing: computational approaches with experimental support, Comput. Mech. 57 (4) (2016) 583–610.
- [2] Y. Zhang, G. Guillemot, M. Bernacki, M. Bellet, Macroscopic thermal finite element modeling of additive metal manufacturing by selective laser melting process, Comput. Methods Appl. Mech. Engrg. 331 (2018) 514–535.
- [3] D. Gu, B. He, Finite element simulation and experimental investigation of residual stresses in selective laser melted Ti–Ni shape memory alloy, Comput. Mater. Sci. 117 (2016) 221–232.
- [4] D. Riedlbauer, T. Scharowsky, R.F. Singer, P. Steinmann, C. Körner, J. Mergheim, Macroscopic simulation and experimental measurement of melt pool characteristics in selective electron beam melting of Ti-6Al-4V, Int. J. Adv. Manuf. Technol. 88 (5–8) (2017) 1309–1317.
- [5] T. Mukherjee, H. Wei, A. De, T. DebRoy, Heat and fluid flow in additive manufacturing—Part I: Modeling of powder bed fusion, Comput. Mater. Sci. 150 (2018) 304–313.
- [6] Q. Chen, G. Guillemot, C.-A. Gandin, M. Bellet, Three-dimensional finite element thermomechanical modeling of additive manufacturing by selective laser melting for ceramic materials, Addit. Manuf. 16 (2017) 124–137.
- [7] Z. Gan, G. Yu, X. He, S. Li, Numerical simulation of thermal behavior and multicomponent mass transfer in direct laser deposition of Co-base alloy on steel, Int. J. Heat Mass Transfer 104 (2017) 28–38.
- [8] W. Yan, W. Ge, Y. Qian, S. Lin, B. Zhou, W.K. Liu, F. Lin, G.J. Wagner, Multi-physics modeling of single/multiple-track defect mechanisms in electron beam selective melting, Acta Mater. 134 (2017) 324–333.
- [9] Z. Gan, Y. Lian, S.E. Lin, K.K. Jones, W.K. Liu, G.J. Wagner, Benchmark study of thermal behavior, surface topography, and dendritic microstructure in selective laser melting of inconel 625, Integrating Mater. Manuf. Innov. 8 (2) (2019) 178–193.
- [10] P. Holmes, J.L. Lumley, G. Berkooz, C.W. Rowley, Turbulence, Coherent Structures, Dynamical Systems and Symmetry, Cambridge university press, 2012.
- [11] P. Kerfriden, O. Goury, T. Rabczuk, S.P.-A. Bordas, A partitioned model order reduction approach to rationalise computational expenses in nonlinear fracture mechanics, Comput. Methods Appl. Mech. Engrg. 256 (2013) 169–188.
- [12] O. Goury, D. Amsallem, S.P.A. Bordas, W.K. Liu, P. Kerfriden, Automatised selection of load paths to construct reduced-order models in computational damage micromechanics: from dissipation-driven random selection to Bayesian optimization, Comput. Mech. 58 (2) (2016) 213–234.
- [13] A. Ammar, B. Mokdad, F. Chinesta, R. Keunings, A new family of solvers for some classes of multidimensional partial differential equations encountered in kinetic theory modeling of complex fluids, J. Non-Newton. Fluid Mech. 139 (3) (2006) 153–176.
- [14] F. Chinesta, P. Ladeveze, E. Cueto, A short review on model order reduction based on proper generalized decomposition, Arch. Comput. Methods Eng. 18 (4) (2011) 395.
- [15] D. Néron, P. Ladevèze, Proper generalized decomposition for multiscale and multiphysics problems, Arch. Comput. Methods Eng. 17 (4) (2010) 351–372.
- [16] S. Niroomandi, I. Alfaro, E. Cueto, F. Chinesta, Model order reduction for hyperelastic materials, Internat. J. Numer. Methods Engrg. 81 (9) (2010) 1180–1206.
- [17] S. Niroomandi, I. Alfaro, D. González, E. Cueto, F. Chinesta, Model order reduction in hyperelasticity: a proper generalized decomposition approach, Internat. J. Numer. Methods Engrg. 96 (3) (2013) 129–149.
- [18] P. Astrid, S. Weiland, K. Willcox, T. Backx, Missing point estimation in models described by proper orthogonal decomposition, IEEE Trans. Automat. Control 53 (10) (2008) 2237–2251.
- [19] D. Ryckelynck, Hyper-reduction of mechanical models involving internal variables, Internat. J. Numer. Methods Engrg. 77 (1) (2009) 75–89.
- [20] S. Chaturantabut, D.C. Sorensen, Nonlinear model reduction via discrete empirical interpolation, SIAM J. Sci. Comput. 32 (5) (2010) 2737–2764.
- [21] F. Fritzen, B. Haasdonk, D. Ryckelynck, S. Schöps, An algorithmic comparison of the hyper-reduction and the discrete empirical interpolation method for a nonlinear thermal problem, Math. Comput. Appl. 23 (1) (2018) 8.
- [22] A. Cosimo, A. Cardona, S. Idelsohn, Global–local ROM for the solution of parabolic problems with highly concentrated moving sources, Comput. Methods Appl. Mech. Engrg. 326 (2017) 739–756.
- [23] Y. Zhang, A. Combescure, A. Gravouil, Efficient hyper-reduced-order model (HROM) for thermal analysis in the moving frame, Internat. J. Numer. Methods Engrg. 111 (2) (2017) 176–200.
- [24] D. Canales, A. Leygue, F. Chinesta, D. González, E. Cueto, E. Feulvarch, J.-M. Bergheau, A. Huerta, Vademecum-based GFEM (V-GFEM): optimal enrichment for transient problems, Internat. J. Numer. Methods Engrg. 108 (9) (2016) 971–989.
- [25] A. Cosimo, A. Cardona, S. Idelsohn, Global-local HROM for non-linear thermal problems with irreversible changes of material states, C. R. Méc. 346 (7) (2018) 539–555.

- [26] Y. Lu, N. Blal, A. Gravouil, Space-time POD based computational vademecums for parametric studies: application to thermo-mechanical problems, Adv. Model. Simul. Eng. Sci. 5 (1) (2018) 3.
- [27] Y. Lu, N. Blal, A. Gravouil, Multi-parametric space-time computational vademecum for parametric studies: Application to real time welding simulations, Finite Elem. Anal. Des. 139 (2018) 62–72.
- [28] Y. Lu, N. Blal, A. Gravouil, Adaptive sparse grid based HOPGD: Toward a nonintrusive strategy for constructing space-time welding computational vademecum, Internat. J. Numer. Methods Engrg. 114 (13) (2018) 1438–1461.
- [29] Y. Lu, N. Blal, A. Gravouil, Datadriven HOPGD based computational vademecum for welding parameter identification, Comput. Mech. 64 (1) (2019) 47–62.
- [30] D. Amsallem, C. Farhat, Interpolation method for adapting reduced-order models and application to aeroelasticity, AIAA J. 46 (7) (2008) 1803–1813.
- [31] R. Mosquera, A. Hamdouni, A. El Hamidi, C. Allery, POD basis interpolation via inverse distance weighting on Grassmann manifolds, Discrete Contin. Dyn. Syst. Ser. S 12 (6) (2019) 1743.
- [32] B. Peherstorfer, K. Willcox, Dynamic data-driven model reduction: adapting reduced models from incomplete data, Adv. Model. Simul. Eng. Sci. 3 (1) (2016) 1–22.
- [33] D. Ryckelynck, A priori hyperreduction method: an adaptive approach, J. Comput. Phys. 202 (1) (2005) 346-366.
- [34] P. Kerfriden, P. Gosselet, S. Adhikari, S.P.-A. Bordas, Bridging proper orthogonal decomposition methods and augmented Newton–Krylov algorithms: an adaptive model order reduction for highly nonlinear mechanical problems, Comput. Methods Appl. Mech. Engrg. 200 (5–8) (2011) 850–866.
- [35] G. Knapp, T. Mukherjee, J. Zuback, H. Wei, T. Palmer, A. De, T. DebRoy, Building blocks for a digital twin of additive manufacturing, Acta Mater. 135 (2017) 390–399.
- [36] S. Patankar, Numerical Heat Transfer and Fluid Flow, Taylor & Francis, 2018.
- [37] J. Fauque, I. Ramière, D. Ryckelynck, Hybrid hyper-reduced modeling for contact mechanics problems, Internat. J. Numer. Methods Engrg. 115 (1) (2018) 117–139.
- [38] T. Maquart, Y. Wenfeng, T. Elguedj, A. Gravouil, M. Rochette, 3D volumetric isotopological meshing for finite element and isogeometric based reduced order modeling, Comput. Methods Appl. Mech. Engrg. 362 (2020) 112809.
- [39] R. Everson, L. Sirovich, Karhunen-Loeve procedure for gappy data, J. Opt. Soc. Amer. A 12 (8) (1995) 1657-1664.
- [40] E. Koronaki, P.A. Gkinis, L. Beex, S.P. Bordas, C. Theodoropoulos, A.G. Boudouvis, Classification of states and model order reduction of large scale chemical vapor deposition processes with solution multiplicity, Comput. Chem. Eng. 121 (2019) 148–157.
- [41] S. Claus, S. Bigot, P. Kerfriden, CutFEM method for Stefan-Signorini problems with application in pulsed laser ablation, SIAM J. Sci. Comput. 40 (5) (2018) B1444-B1469.